The Ska complex promotes Aurora B activity to ensure chromosome biorientation

Patrick M. Redli,[1] Ivana Gasic,[2] Patrick Meraldi,[2] Erich A. Nigg,[1] and Anna Santamaria[1,3]

[1]Growth and Development, Biozentrum, University of Basel, 4056 Basel, Switzerland
[2]Department of Cell Physiology and Metabolism, Medical Faculty, University of Geneva, 1211 Geneva, Switzerland
[3]Cell Cycle and Cancer, Group of Biomedical Research in Gynecology, Vall d'Hebron Research Institute (VHIR)-UAB, 08035 Barcelona, Spain

Chromosome biorientation and accurate segregation rely on the plasticity of kinetochore–microtubule (KT-MT) attachments. Aurora B facilitates KT-MT dynamics by phosphorylating kinetochore proteins that are critical for KT-MT interactions. Among the substrates whose microtubule and kinetochore binding is curtailed by Aurora B is the spindle and kinetochore-associated (Ska) complex, a key factor for KT-MT stability. Here, we show that Ska is not only a substrate of Aurora B, but is also required for Aurora B activity. Ska-deficient cells fail to biorient and display chromosome segregation errors underlying suppressed KT-MT turnover. These defects coincide with KNL1–Mis12–Ndc80 network hypophosphorylation, reduced mitotic centromere-associated kinesin localization, and Aurora B T-loop phosphorylation at kinetochores. We further show that Ska requires its microtubule-binding capability to promote Aurora B activity in cells and stimulates Aurora B catalytic activity in vitro. Finally, we show that protein phosphatase 1 counteracts Aurora B activity to enable Ska kinetochore accumulation once biorientation is achieved. We propose that Ska promotes Aurora B activity to limit its own microtubule and kinetochore association and to ensure that KT-MT dynamics and stability fall within an optimal balance for biorientation.

Introduction

Proper chromosome attachment to opposite spindle poles (biorientation) and error-free chromosome segregation rely on the plasticity of kinetochore–microtubule (KT-MT) attachments; these must remain flexible enough to allow the release of erroneously attached spindle MTs, yet become sufficiently stable to harness forces for chromosome movements and silence the spindle assembly checkpoint (SAC). To achieve this dynamic range, both the strength of the grip of KTs on the MT lattice and the turnover of KT-MT plus ends within the KT binding sites must be finely regulated during the course of mitosis. Failure in this regulation can give rise to chromosomal instability, a common feature of most solid tumors (Lengauer et al., 1998; Thompson et al., 2010; Bakhoum and Compton, 2012). Thus, identifying the molecular players and understanding the mechanisms that govern the fine-tuning and coordination of the stability and dynamics of KT-MTs is an important task.

One of the key regulators of both KT-MT attachment stability and plus-end dynamics is the conserved serine/threonine kinase Aurora B (Ditchfield et al., 2003; Hauf et al., 2003; Cimini et al., 2006; Muñoz-Barrera and Monje-Casas, 2014). Before anaphase, Aurora B is found along chromosome arms and becomes enriched at the inner centromere as part of the chromosomal passenger complex (CPC), which also includes Borealin, the inner centromere protein (INCENP), and Survivin (Carmena et al., 2012). Functionally relevant pools of the kinase or its phosphorylated forms have also been reported to localize to spindle MTs (Tseng et al., 2010; Banerjee et al., 2014; Krupina et al., 2016) and KTs before anaphase (Posch et al., 2010; DeLuca et al., 2011; Petsalaki et al., 2011; Bekier et al., 2015). At KTs, Aurora B phosphorylates outer KT proteins that bind MTs, including the KNL1–Mis12–Ndc80 (KMN) network and the spindle and KT-associated (Ska) complex, to decrease their MT-binding activity and actively promote MT catastrophe (Lampson et al., 2004; Welburn et al., 2010; Chan et al., 2012; Schmidt et al., 2012; Umbreit et al., 2012; Sarangapani et al., 2013). Moreover, the kinase regulates KT-MT dynamics by controlling the localization and activity of various MT-associated proteins, such as the MT-depolymerizing mitotic centromere-associated kinesin (MCAK; Andrews et al., 2004; Lan et al., 2004; Wordeman et al., 2007; Bakhoum et al., 2009). Finally, Aurora B opposes protein phosphatases, including protein phosphatase 1 (PP1) and PP2A-B56 families,

Correspondence to Anna Santamaria: anna.santamaria@vhir.org

I. Gasic's present address is Dept. of Systems Biology, Harvard Medical School, Boston, MA 02115.

Abbreviations used: CB^{DBD}, CENP-B-DNA-binding domain; CPC, chromosomal passenger complex; FRET, fluorescence resonance energy transfer; INCENP, inner centromere protein; K-fiber, kinetochore-fiber; KMN, KNL1–Mis12–Ndc80; KT, kinetochore; MBP, maltose-binding protein; MCAK, mitotic centromere-associated kinesin; MT, microtubule; MTBD, microtubule-binding domain; OA, okadaic acid; PA, photoactivatable; PP1, protein phosphatase 1; SAC, spindle assembly checkpoint; ZM, ZM447439.

The Rockefeller University Press $30.00
J. Cell Biol. Vol. 215 No. 1 77–93
www.jcb.org/cgi/doi/10.1083/jcb.201603019

which, in turn, counteract the phosphorylation of Aurora B substrates and negatively regulate Aurora B activity (Francisco et al., 1994; Hsu et al., 2000; Liu et al., 2010; Foley et al., 2011; Krenn and Musacchio, 2015). These Aurora B functions prevent accumulation of attachment errors during establishment of biorientation in early mitosis and sustain an adequate degree of KT-MT attachment dynamics to ensure a high responsiveness for error correction as well as fluid KT-MT plus-end turnover for chromosome movements in late mitosis (Cimini et al., 2006; DeLuca et al., 2011).

Among the various KT targets of Aurora B, the Ska complex is recognized as an important factor for kinetochore-fiber (K-fiber) stability and as a potential functional equivalent of the yeast Dam1 complex that couples chromosome movement to MT plus-end depolymerization (Hanisch et al., 2006; Gaitanos et al., 2009; Raaijmakers et al., 2009; Welburn et al., 2009; Schmidt et al., 2012). The tripartite complex (Ska1, Ska2, and Ska3) localizes and binds to both spindle MTs and outer KTs after nuclear envelope breakdown. While it stays associated with spindle MTs throughout mitosis, the complex becomes maximally enriched at bioriented KTs in late prometaphase/metaphase and leaves the KTs in telophase (Raaijmakers et al., 2009; Chan et al., 2012; Jeyaprakash et al., 2012). Accumulation of Ska at the KT-MT interface confers cold stability to K-fibers, and this function is opposed by Aurora B activity (Chan et al., 2012). Ska has been also implicated in chromosome congression and timely metaphase-to-anaphase transition (Hanisch et al., 2006; Schmidt et al., 2012; Abad et al., 2014). The latter possibly reflects a role of Ska in silencing the SAC via PP1 recruitment (Sivakumar et al., 2016) or in facilitating the activity of the anaphase-promoting complex/cyclosome (Daum et al., 2009; Sivakumar et al., 2014).

Here, we focus on the functional interaction between the Ska complex and Aurora B kinase and show that the Ska complex is required not only for K-fiber stability but also for chromosome biorientation and control of KT-MT dynamics by promoting Aurora B activity. Our results lead us to propose a feedback mechanism in which stimulation of Aurora B activity by the Ska complex during biorientation limits Ska accumulation at KTs and/or the spindle, sustaining a high degree of KT-MT dynamics. At bioriented chromosomes, this regulation is antagonized by PP1, allowing accumulation of Ska and stabilization of proper KT-MT attachments.

Results

The Ska complex is required for error-free chromosome segregation and regulation of KT-MT dynamics

To gain novel insights into Ska complex function, we used high-resolution time-lapse microscopy to reexplore the consequences of Ska depletion in HeLa S3 cells stably expressing histone H2B–GFP that were cotransfected with siRNAs against two Ska subunits (Ska1 and Ska3). As reported previously (Hanisch et al., 2006; Daum et al., 2009; Gaitanos et al., 2009; Welburn et al., 2009), Ska-depleted cells displayed prominent early mitotic defects, including (a) a late-prometaphase delay with occasional loss of chromosomes from the spindle equator and rotation and/or widening of the equatorial plate, (b) a similar late-prometaphase state with subsequent chromosome scattering (cohesion fatigue), and (c) a complete chromosome congression failure (Fig. S1 A). Whereas cells showing chromosome scattering and alignment defects underwent mitotic cell death in the majority of cases (Gaitanos et al., 2009), the surviving cells (50–75% of the total population) eventually progressed into anaphase. Interestingly, when we analyzed chromosome behavior in these cells, we observed a marked increase in the frequency of segregation errors. Specifically, 21% of Ska-depleted cells in anaphase displayed lagging chromosomes, compared with 3% of control cells (Fig. 1, A and B). Chromatin bridges were also detected at lower but elevated frequencies (10% vs. 4% for Ska depletion and control cells, respectively; Fig. S1, B and C). Live-cell analysis showed that lagging chromosomes occasionally segregated, either as whole chromosomes or as fragments after chromosome breakage, into micronuclei (unpublished data). Consistently, micronucleated cells occurred with a twofold higher frequency when measured in fixed cells (11% for Ska-depleted vs. 5% for control cells; Fig. 1, C and D). Based on the assumption that single lagging chromosomes and micronuclei arise primarily from persistent merotelic attachments (where a single KT is attached to both spindle poles; Cimini et al., 2001, 2002; Thompson and Compton, 2011), we scored as an estimate for the frequency of merotelic attachment in late prometaphase, the percentage of cells with lagging single KTs, as well as the number of single lagging KTs per anaphase (seen as single unpaired EGFP-CENP-A dots) in a live-cell assay with stable HeLa K EGFP-CENP-A cells, in which we added reversine upon chromosome alignment to force premature anaphase entry (Salmon et al., 2005). Under this condition, both the percentage of anaphase cells with single lagging KTs and the number of single lagging KTs per cell was higher in Ska-deficient cells, indicating the prevalence of merotelic malorientations (Fig. 1 E and Fig. S1, D and E). Together, these data suggest a role of the Ska complex in correction or prevention of merotelic attachments, thus revealing a novel phenotypic aspect of Ska loss-of-function.

To test whether the Ska complex promotes error correction by modulating KT-MT dynamics, we examined MT plus-end turnover after Ska complex depletion (by Ska3 single-siRNA treatment) in HeLa K cells stably expressing photoactivatable (PA) GFP–α-tubulin (Amaro et al., 2010; see Fig. S1, F and G, for knockdown efficiency and cell viability comparable to those seen in HeLa S3 cells). Tubulin turnover at MT plus ends was measured by fluorescence dissipation after GFP photoactivation (Fig. 1, F and G; Materials and methods). Knockdown of the Ska complex increased the fraction of non–KT-MTs (from 52% in control cells to 67% in Ska3-depleted cells; Fig. 1 H), in line with previous cold-sensitivity assays (Hanisch et al., 2006; Gaitanos et al., 2009). Moreover, Ska deficiency caused a ∼1.8-fold increase in the half-life of KT-MTs relative to control-depleted cells (368 vs. 202 s for siSka3 and control cells, respectively), whereas half-lives of non–KT-MTs remained similar (14 vs. 12 s for siSka3 and control cells, respectively; Fig. 1 I). Comparable results were obtained when targeting the Ska complex with Ska1 single-siRNA treatment (Fig. S1 H). We conclude that depletion of the Ska complex results in fewer yet more stable K-fibers, a situation that may impair error correction and favor lagging chromosomes.

The Ska complex is required for Aurora B activity

The Ska complex has been identified as an Aurora B substrate (Chan et al., 2012). Now we find that several phenotypes

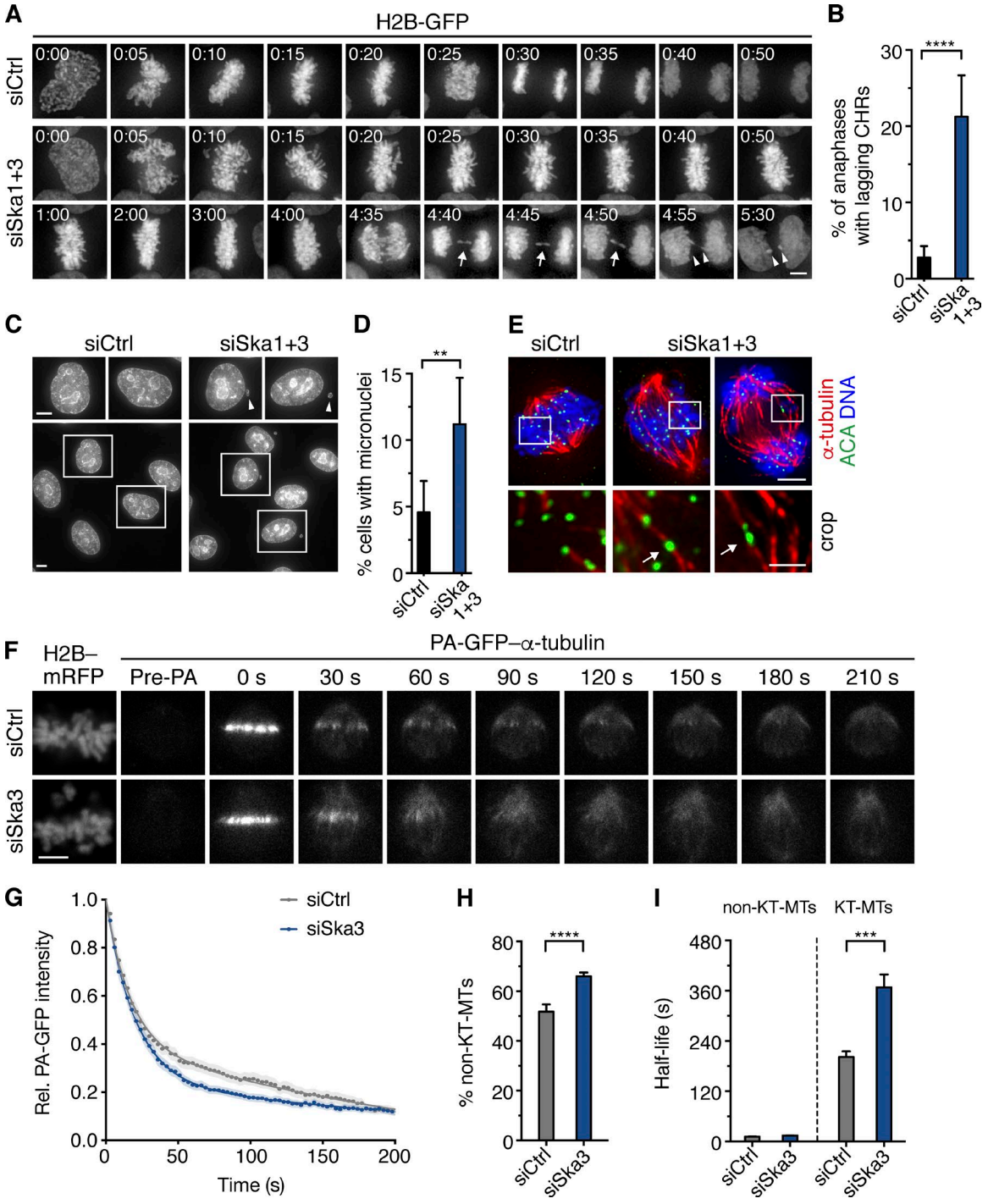

Figure 1. **The Ska complex is required for error-free chromosome segregation and regulation of KT-MT dynamics.** (A) Stills from live-imaging videos of HeLa S3 H2B–GFP cells treated with control or Ska1 and Ska3 siRNAs for 36–40 h before filming. Arrows point at the lagging chromosome; arrowheads highlight chromosome fragments. (B) Percentage of anaphase cells with lagging chromosomes (CHRs). Bars represent mean ± 95% CI ($n \geq 300$ anaphase cells per condition from four independent experiments). (C) Nuclear integrity of siControl or siSka1+3 cells in interphase 48 h after siRNA transfection. (D) Percentage of micronucleated interphase cells. Bars represent mean ± 95% CI (n = 1,500 cells per condition from three experiments). (E) siControl or siSka1+3 transfected cells were treated after 48 h with the Mps1 inhibitor reversine for 20–25 min to force anaphase entry, followed by 5-min incubation at 4°C to depolymerize non-KT-MTs. Cells were fixed and stained with the indicated antibodies. Shown are optical sections of a siControl cell (left) with a bioriented sister KT pair in the enlarged crop before anaphase onset, and siSka1+3 cells (right) with merotelic KTs highlighted with arrows before and after anaphase onset. (F) Live-cell fluorescence images before and after photoactivation of HeLa K cells stably expressing PA-GFP–α-tubulin/H2B–mRFP treated with control or Ska3 siRNAs for 48 h. Note that depletion of a single Ska subunits leads to complete loss of the complex (see Fig. S1 G). (G) Quantification of the fluorescence intensity decay of the activated regions over time. Relative GFP intensities were fitted to a double exponential equation corresponding to fast (non-KT-MT) and slow (KT-MT) MT populations (see Materials and methods for details and Table S1 for sample sizes and fitting parameters). Shaded areas represent the 95% CI. Percentage of the non-KT-MTs (H) and half-lives of non-KT-MTs and KT-MTs (I) obtained from G. Bars represent mean ± 95% CI. Asterisks show statistical significance (Student's *t* test, unpaired). ****, $P \leq 0.0001$; ***, $P \leq 0.001$; **, $P \leq 0.01$. Bars: 5 µm; (E, bottom) 1 µm.

observed after Ska depletion (i.e., lagging chromosomes/merotelic KT malorientations and suppressed KT-MT plus-end turnover) are reminiscent of described consequences of Aurora B loss-of-function (Cimini et al., 2006; DeLuca et al., 2011). Hence, we reasoned that the Ska complex might control KT-MT plus-end turnover via Aurora B. To determine whether Aurora B activity depends on Ska, we first examined established Aurora B KT substrates that regulate interactions with MTs (Cheeseman et al., 2006; DeLuca et al., 2006, 2011; Welburn et al., 2010). Phosphorylation of KMN network substrates, namely serine 44 on Hec1 (Hec1-pS44), serine 24 on KNL1 (KNL1-pS24), and serine 100 on Dsn1 (Dsn1-pS100), was significantly reduced in both late-prometaphase (Fig. 2, A–D; and Fig. S2, A–C) and early-prometaphase (not depicted) cells after Ska depletion. Likewise, inner KT enrichment but not spindle pole association of MCAK, an Aurora B effector implicated in the regulation of KT-MT plus-end dynamics (Bakhoum et al., 2009; Tanno et al., 2010), was diminished (Fig. 2, E and F). We also observed a decrease in the phosphorylation of histone H3 on both serine 10 (H3-pS10) and serine 28 (H3-pS28), an Aurora B substrate localizing along chromosome arms (Goto et al., 2002), when targeting the Ska complex with siRNAs against Ska1 and Ska3 (Fig. 2, G and H; and Fig. S2, D and E). Similar results were obtained with a panel of different siRNAs (Fig. S2, F and G), and complementation of the depleted Ska complex subunits partially rescued H3-S10 phosphorylation (Fig. 2, I and J), attesting to specificity. Treatment of Ska-depleted cells with the PP1 and PP2 inhibitor okadaic acid (OA) did not revert H3-pS10, indicating that this effect is not caused by phosphatase mistargeting from KTs (Sivakumar et al., 2016; unpublished data). Finally, Ska knockdown also suppressed Aurora B phosphorylation in living HeLa K cells stably expressing either a CENP-B–fused or a histone H2B–fused fluorescence resonance energy transfer (FRET) sensor for Aurora B activity (Fuller et al., 2008), albeit to a lesser extent than direct inhibition of Aurora B with high concentrations of ZM447439 (ZM; Fig. 2, K–N; and Fig. S2, H and I; see Discussion). We conclude that the Ska complex promotes Aurora B activity to facilitate KT-MT turnover and prevent the accumulation of attachment errors.

The Ska complex promotes Aurora B kinase activity at KTs independently of Aurora B centromere targeting

Next, we sought to determine the underlying molecular mechanism by which the Ska complex promotes Aurora B activity. Previous work suggested that concentration of the CPC at the inner centromere contributes to Aurora B kinase activity by transactivation (Kelly et al., 2007, 2010; Wang et al., 2011). We therefore first examined the localization of CPC subunits in Ska-depleted cells, in which protein levels or complex formation of the CPC was not detectably affected (Fig. S3, A–C). Although the localization of Aurora B and Borealin was less clearly defined at mitotic centromeres and appeared more diffusely distributed on chromatin in Ska-deficient cells with scattered chromosomes (34% of cells with bipolar spindles), cells with aligned chromosomes (66% of cells) showed only a minor decrease in the centromeric enrichment of both proteins (Fig. 3, A and B; and not depicted), arguing against the notion that abrogated CPC centromere recruitment is the primary cause for the observed defects in Aurora B substrate phosphorylation.

Notably, we also found that CPC displacement from centromeres correlated not only with the alignment status of Ska-depleted cells, but also with a decrease in Haspin kinase-dependent phosphorylation of histone H3 on threonine 3 (H3-pT3; Fig. 3, A and C), a chromatin mark important to target the CPC to the inner centromere (De Antoni et al., 2012; Wang et al., 2012). This finding prompted us to test whether chromosome scattering associated with cohesion fatigue (Daum et al., 2009; Sivakumar et al., 2014) or perturbed Haspin function may contribute to the decreased Aurora B activity levels in Ska-depleted cells, but we found that neither induction of cohesion fatigue (Fig. S3, D–G) nor direct Haspin inhibition (Fig. S3, H–J) lowered Aurora B activity toward histone H3-S10.

To assess whether the impairment of Aurora B function in Ska-deficient cells was a result of perturbation of Aurora B kinase activity, we next monitored the levels of active Aurora B using phosphospecific antibodies against the Aurora B activation loop (AurB-pT232; Yasui et al., 2004; DeLuca et al., 2011). To exclude effects caused by changes in bulk localization of Aurora B at centromeres, we focused our analysis on Ska-deficient cells with aligned chromosomes and costained the cells with Aurora B antibodies recognizing nonphosphorylated epitopes. We found that the extent of Aurora B–T232 phosphorylation at KTs was significantly reduced (Fig. 3, D and E), indicating that the Ska complex promotes Aurora B kinase activity at KTs.

To further corroborate that the Ska complex regulates Aurora B activity independently of its centromere enrichment, we forced Aurora B accumulation at centromeres through expression of a CENP-B-DNA-binding domain (CB^{DBD})-INCENP fusion protein (Liu et al., 2009). Although CB^{DBD}-INCENP targeted to centromeres and drove Aurora B centromere enrichment in Ska-depleted cells as efficiently as in control cells (Fig. 3, F and G), expression of CB^{DBD}-INCENP failed to fully restore Aurora B activation loop phosphorylation (Fig. 3, H and I). Likewise, ectopic targeting of Aurora B to centromeres did not rescue control levels of MCAK KT localization (Fig. S3, K and L) or H3-S10 phosphorylation (Fig. S3, M and N). Collectively, these data suggest that the Ska complex enhances Aurora B kinase activity at both KTs and chromosome arms largely independently of its centromere localization.

The Ska complex promotes Aurora B activity in an MT-dependent manner

Most of the functions of the Ska complex have been linked to its ability to directly associate with spindle MTs. To see whether the Ska complex also requires its MT-binding capability to promote Aurora B kinase activity, we depleted endogenous Ska1 in HeLa cells stably expressing mutant versions of RNAi-resistant GFP-Ska1 lacking either a basic patch in the MT-binding surface of Ska1 ($Ska1^{R155A,\ R236A,\ R245A}$) or the entire MT-binding domain (MTBD; $Ska1^{\Delta MTBD}$; residues 1–131; see Fig. S4 A for expression levels of the different Ska rescue constructs; Schmidt et al., 2012). These mutants both make the full Ska complex MT-binding deficient in vitro without affecting complex formation; in intact cells, they fail to localize to spindle MTs but not KTs (Schmidt et al., 2012; Abad et al., 2014). Although Ska1-depleted cells expressing wild-type Ska1 showed Hec1-pS44, KNL1-pS24, MCAK KT, H3-pS10, and Aurora B–pT232 levels comparable to those of control cells, expression of $Ska1^{R155A,\ R236A,\ R245A}$ and $Ska1^{\Delta MTBD}$ failed to restore wild-type levels of these Aurora B activity markers (Fig. 4). These results indicate that the Ska complex regulates Aurora B activity in an MT-dependent manner.

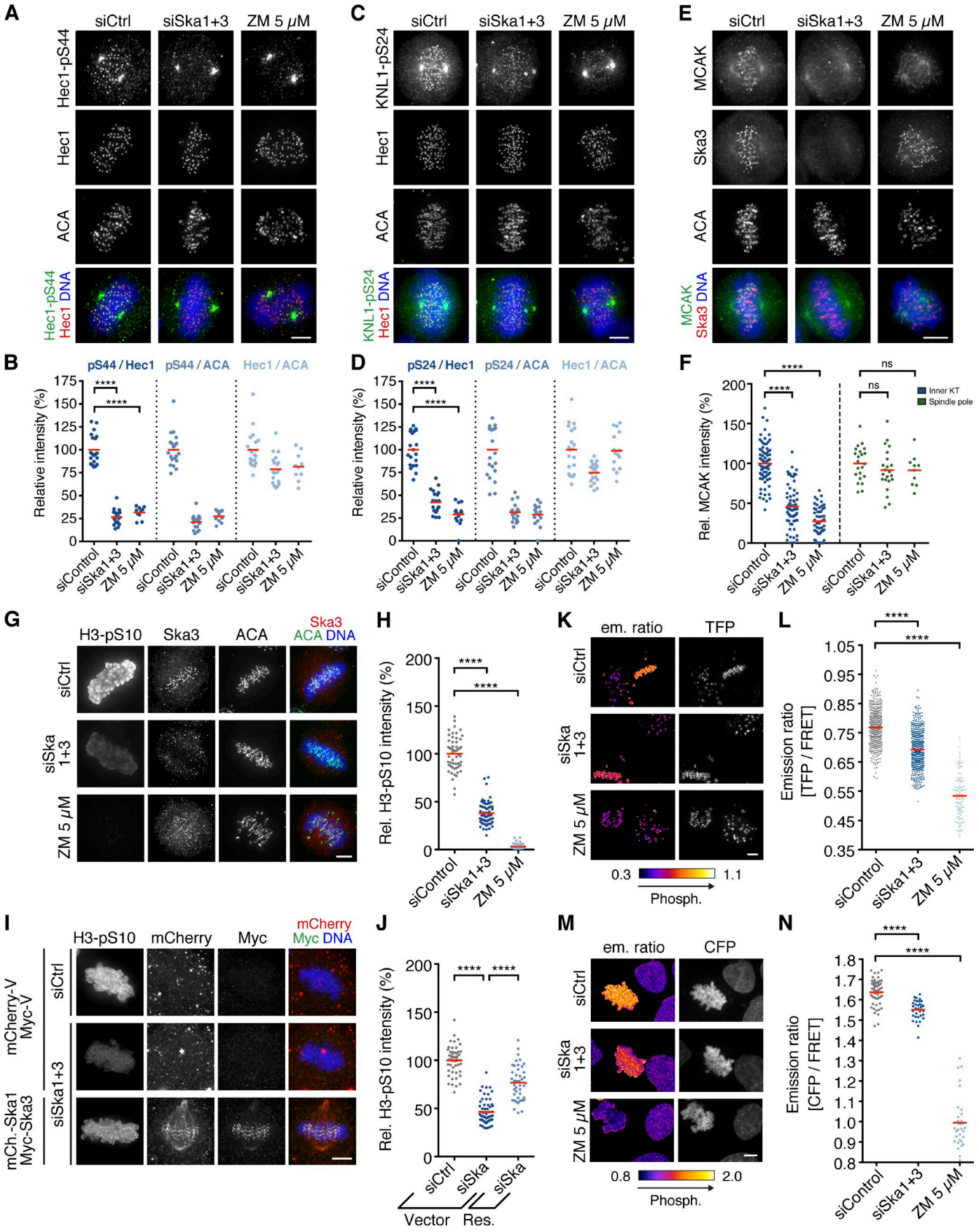

Figure 2. **The Ska complex is required for Aurora B activity in cells.** Immunofluorescence images (A, C, E, and G) and quantification (B, D, F, and H) of relative Hec1-pS44, KNL1-pS24, MCAK, and histone H3-pS10 intensities, respectively, in HeLa S3 cells treated for 48 h with control or Ska1 and Ska3 siRNAs. The Aurora B inhibitor ZM was added to siControl cells 1 h before fixation (n = 10–20, n = 15–20, n = 10–77, and n = 47–61 cells per condition, respectively, from one to three experiments). (I) HeLa S3 cells were depleted of endogenous Ska1 and Ska3 or treated with control siRNAs, synchronized

To further explore a dependence on MTs, we examined H3-S10 phosphorylation in Ska-depleted cells that had been treated with high doses of nocodazole before mitotic entry (Fig. S4 B). Under these conditions, the Ska complex was dispensable for H3-S10 phosphorylation (Fig. S4 C). Notably, however, levels of H3-pS10 were significantly lower after premitotic nocodazole treatment compared with DMSO-treated prometaphase cells (Fig. S4 C), consistent with a requirement of spindle MTs for Aurora B activation in prometaphase (Banerjee et al., 2014). In further support of this notion, we found that when mitotic cells in which Aurora B was initially inhibited with ZM, but reactivation of the kinase was allowed upon washout of the inhibitor, Aurora B activity toward histone H3-pS10 recovered faster in the presence of MTs (namely in taxol or upon nocodazole washout) and absence of Aurora B centromere enrichment (when Haspin was inhibited; Fig. S4, D and E). This suggests that spindle MTs can contribute to Aurora B activity also independently of facilitating its centromere targeting (Banerjee et al., 2014). Collectively, these results support the hypothesis that spindle MTs facilitate Aurora B activation and that the Ska complex, in turn, depends on MTs to functionally interact with Aurora B.

The Ska complex stimulates Aurora B kinase activity in vitro

Finally, we asked whether the Ska complex could directly promote the catalytic activity of Aurora B. To test this hypothesis, we examined Aurora B activation in vitro (Fig. 5 A and Fig. S5 A). Aurora B was preincubated in the presence of its primary activator, the INCENP IN-Box domain (INCENP$^{790–919}$), with the reconstituted Ska complex or equimolar amounts of BSA (as negative control for molecular crowding) before γ-[^{32}P] ATP and recombinant histone H3 as substrate were added to initiate the kinase reaction. Compared with preincubation with BSA, the Ska complex markedly enhanced the rate of histone H3 phosphorylation (Fig. 5, A and B) as well as Aurora B autophosphorylation (Fig. S5 B). Similar results were obtained when BSA was omitted (Fig. S5 C), and BSA had a negligible effect on Aurora B autophosphorylation (Fig. S5 D), ruling out that BSA interfered with Aurora B activation. Likewise, incubation of the Ska complex with γ-[^{32}P]ATP and histone H3, but without Aurora B and INCENP$^{790–918}$, did not increase incorporation of ^{32}P into histone H3, confirming the absence of copurifying bacterial kinases (Fig. S5 E). Together, these results show that the Ska complex is able to stimulate the kinase activity of Aurora B within the CPC core complex. They further suggest that Ska directly interacts with the CPC core complex. Consistently, the Ska complex associated with Aurora B in vitro (Fig. 5 C), and we reproducibly found the CPC subunits Aurora B, INCENP, and Survivin in endogenous Ska1 immunoprecipitates from mitotic HeLa S3 cells (Fig. 5 D). However, we failed to clearly detect Ska complex subunits in reverse immunoprecipitation assays using INCENP or Aurora B antibodies (Figs. S3 C and S5 F), possibly reflecting differences in the abundance of the binding partners or steric hindrance by antibodies.

Having shown that Ska directly associates with Aurora B, we further asked whether the Ska complex could promote Aurora B activity independently of INCENP$^{790–918}$. Incubation of increasing amounts of the Ska complex with Aurora B enhanced kinase autophosphorylation in a dose-dependent fashion. In comparison, incubation with histone H3 (as control) led to only a marginal increase in Aurora B ^{32}P incorporation, presumably reflecting an nonspecific stimulation of Aurora B autophosphorylation (Fig. 5, E and F; and Fig. S5 G). Similar results were obtained in a time course assay in which histone H3 was replaced with a buffer control to exclude a possible inhibitory effect of histone H3 on Aurora B activity (Fig. S5, H and I; Rosasco-Nitcher et al., 2008). A time course assay with Aurora B and the Ska complex in the presence of histone H3 as substrate further revealed that the observed Ska-dependent increase in Aurora B autophosphorylation translated into an up to threefold higher histone H3 phosphorylation efficiency relative to BSA (Fig. 5, G and H). In comparison, INCENP$^{790–919}$ stimulated H3 phosphorylation up to sixfold (Fig. 5, G and H). Finally, we tested whether any of the three Ska complex components could individually promote Aurora B catalytic activity and found that, of the two subunits that are also substrates of Aurora B (Chan et al., 2012), Ska1 but not Ska3 dose-dependently promoted Aurora B autophosphorylation (Fig. S5, J and K). We conclude that the Ska complex can directly associate with Aurora B and promote, presumably in a Ska1-mediated fashion, an active conformation or transactivation of Aurora B, without modulating the interaction of the kinase with its primary activator, the INCENP IN-box domain.

PP1 protects the Ska complex from Aurora B phosphorylation to enable its accumulation at bioriented KTs

Previous work has established that timely accumulation of the Ska complex at the KT-MT interface after chromosome biorientation is important for stabilizing K-fibers and that Aurora B opposes this function by lowering the binding affinity of the complex for its outer KT receptor, the KMN network, and MTs (Chan et al., 2012; Jeyaprakash et al., 2012; Schmidt et al., 2012; Abad et al., 2014). The data presented here further suggest that the Ska complex, in turn, promotes Aurora B activity, presumably on the mitotic spindle and/or at KTs (see Discussion). So, how is the Ska complex able to accumulate at the KT-MT interface and stabilize K-fibers upon chromosome biorientation, if it also stimulates the kinase that antagonizes this function? One possibility is that KT recruitment of phosphatases counteracting Aurora B might protect the Ska complex from Aurora B phosphorylation. To test this hypothesis, we arrested HeLa S3 cells in prometaphase using STLC (an Eg5 inhibitor) or in metaphase using MG132 (a proteasome inhibitor), subjected the cells to

by a double thymidine arrest/release, and rescued (Res.) by transfection with siRNA-resistant mCherry (mCh.)-Ska1 and Myc-Ska3 or empty mCherry- and Myc-Vectors (Vector), as control, and stained with the indicated antibodies. (J) Relative H3-pS10 intensities in cells treated as in I (n = 44–59 cells from two experiments). Res., rescue with mCh.-Ska1 and Myc-Ska3. Live-cell images of HeLa K cells stably expressing a CENP-B–fused (K and L) or H2B-fused (M and N) Aurora B FRET sensor treated as in A. The FRET sensors were completely dephosphorylated in siControl cells treated with ZM 30 min before imaging. Shown are emission ratio images (TFP/YFP or CFP/YFP) and images for sensor localization (TFP or CFP emission). (L) Scatter plot showing TFP/YFP emission ratios calculated for individual aligned KTs in siControl and siSka1+3 cells (n = 500 KTs from 50 cells each from two experiments) or mostly unaligned KTs in ZM-treated cells (n = 100 KTs from 10 cells from one experiment). (N) CFP/YFP emission ratios calculated for individual siControl and siSka1+3 cells with aligned chromosomes (n = 33–55 cells from three experiments) or ZM-treated cells with mostly unaligned chromosomes (n = 33 cells from one experiment). Horizontal lines depict mean. Asterisks show statistical significance (Student's t test, unpaired). ****, $P \leq 0.0001$; ns, nonsignificant. Bars, 5 µm.

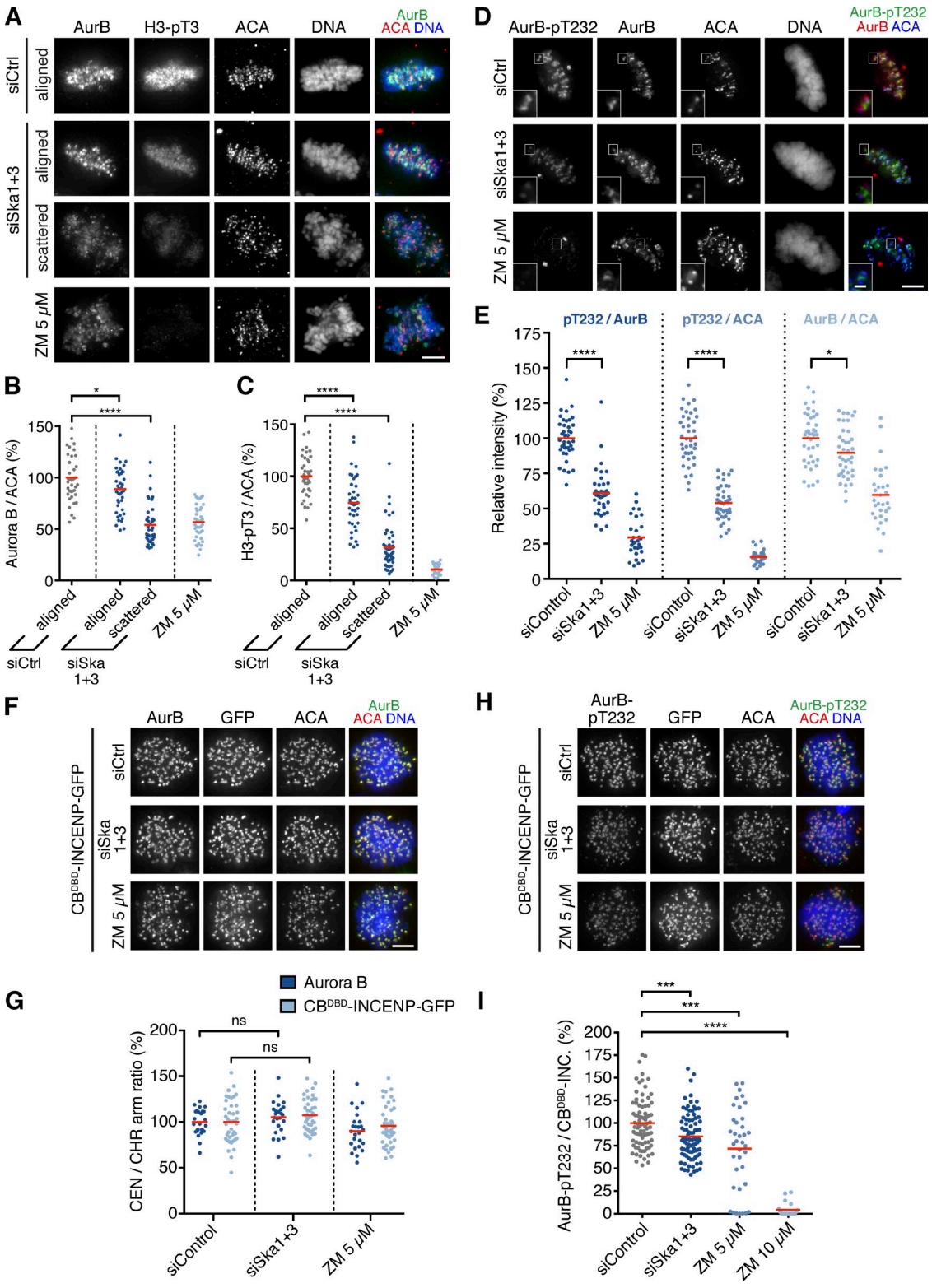

Figure 3. **The Ska complex promotes Aurora B kinase activity at KTs independently of Aurora B centromere targeting.** HeLa S3 cells treated for 48 h with control, Ska1 and Ska3, or control siRNAs and ZM for 1 h were fixed and stained for Aurora B and H3-pT3 (A) or AurB-pT232 (D). (B) Quantification of Aurora B centromere levels (n = 40 cells per condition from three experiments). (C) Relative histone H3-pT3 intensities in cells treated as in A (n = 40 cells per condition from three experiments). (E) Relative AurB-pT232 and Aurora B intensities in cells treated as in D (n = 30–40 per condition from two experiments). (F–I) HeLa S3 cells were cotransfected with CB^{DBD}-INCENP–GFP and control or Ska1 and Ska3 siRNAs for 48 h. ZM was added to siControl cells 1 h before fixation. Immunofluorescence images (F) and quantification (G) of Aurora B and CB^{DBD}-INCENP–GFP centromere (CEN) over chromosome (CHR) arm signal ratios (n = 25–44 cells per condition from two or more experiments). Immunofluorescence images (H) and quantification (I) of AurB-pT232 over CB^{DBD}-INCENP–GFP signal ratios (n = 19–86 cells per condition from one to three experiments). Asterisks show statistical significance (Student's t test, unpaired). ****, P ≤ 0.0001; ***, P ≤ 0.001; *, P ≤ 0.05; ns, nonsignificant. Bars: 5 µm; (D, insets) 1 µm.

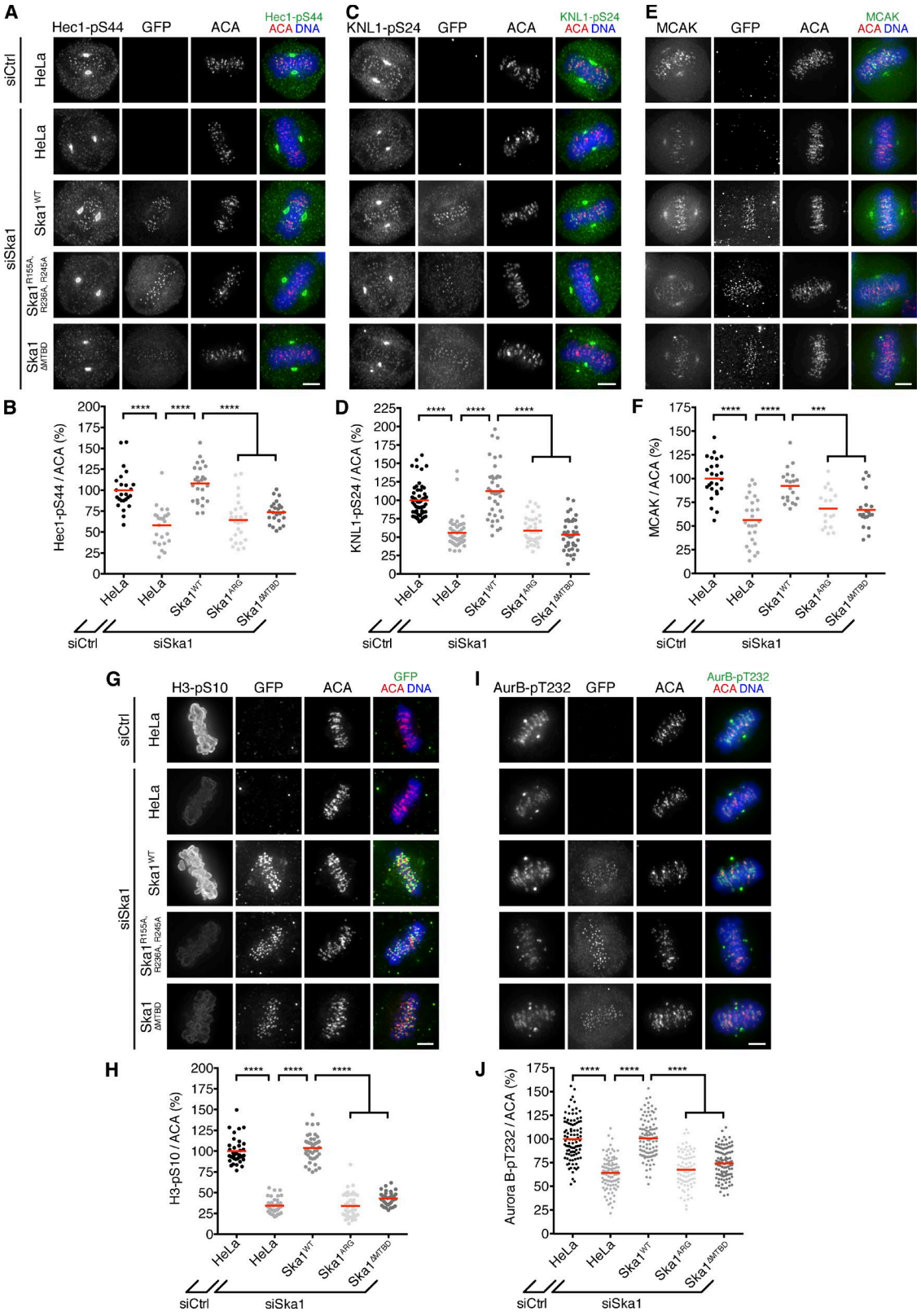

Figure 4. **The MT-binding capability of the Ska complex is required for Aurora B activity.** Immunofluorescence images (A, C, E, G, and I) and quantification (B, D, F, H, and J) of relative Hec1-pS44, KNL1-pS24, MCAK, histone H3-pS10, and AurB-pT232 intensities, respectively, in HeLa cells stably expressing GFP-tagged and siRNA-resistant wild-type Ska1 (WT) or the MT-binding deficient mutants Ska1$^{R155A, R236A, R245A}$ (ARG) and Ska1$^{1-131}$ (ΔMTBD), respectively, treated for 48 h with control or Ska1 siRNAs (n = 25, n = 40–55, n = 17–26, n = 35–40, and n = 81–105 cells per condition, respectively, from one to four experiments). Note that spindle association of GFP-Ska1^{WT} is not visible in all cells because of the simultaneous cell permeabilization and fixation. Horizontal lines depict mean. Asterisks show statistical significance (Student's t test, unpaired). ****, $P \leq 0.0001$; ***, $P \leq 0.001$. Bars, 5 µm.

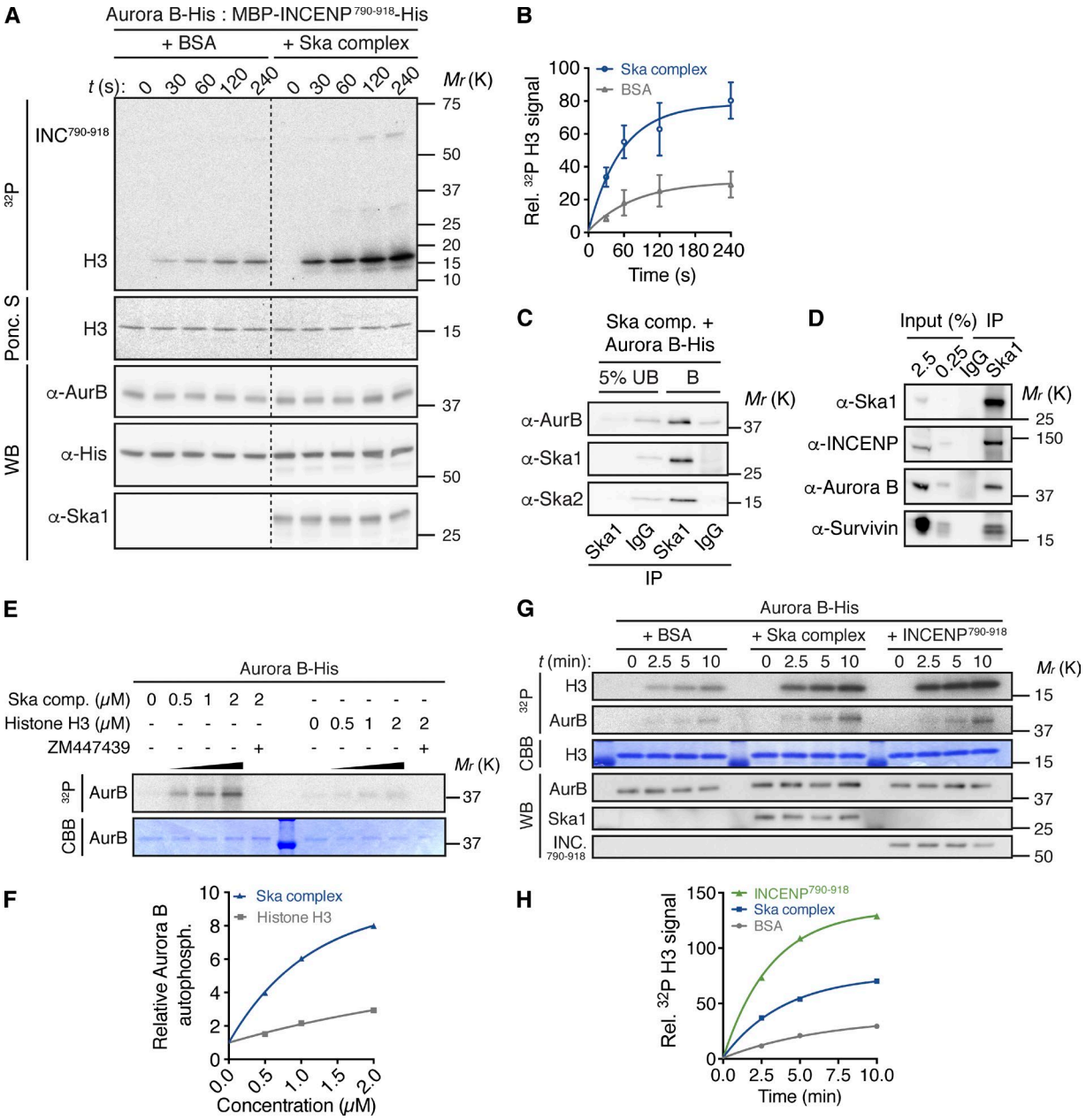

Figure 5. **The Ska complex promotes the catalytic activity of Aurora B in vitro.** (A) Time course kinase assay with Aurora B–His and MBP–INCENP$^{790–919}$–His preincubated with Ska complex or equimolar amounts of BSA, as control, before addition of histone H3 and γ-[^{32}P]ATP. (B) Quantification of histone H3 ^{32}P signals from A. Signals were normalized to H3 and Aurora B protein levels monitored by Ponceau S staining (Ponc. S) and Western blotting (WB), respectively. Signal intensities are expressed relative to the first time-point. Data represent mean ± SD (three experiments). (C) Aurora B–His was incubated with recombinant Ska complex before pull-down with beads coupled to anti-Ska1 antibody or control antibody (IgG). UB, unbound fraction; B, bound fraction. (D) Immunoprecipitates (IP) from mitotic HeLa S3 cell extracts, obtained using anti-Ska1 antibodies or control antibodies (IgG), analyzed by WB. (E) Aurora B–His was preincubated with Ska complex (comp.) or histone H3, as control, before incubation with γ-[^{32}P]ATP. Aurora B autophosphorylation is visualized by autoradiography (^{32}P) and Aurora B levels by Coomassie Brilliant Blue (CBB) staining (see Fig. S5 G for uncropped results). (F) Quantification of Aurora B autophosphorylation signals from E (one experiment). Signal intensities are expressed relative to the first concentration. (G) Time course kinase assay with recombinant Aurora B–His preincubated with Ska complex, equimolar amounts of MBP–INCENP$^{790–919}$–His or BSA, as control, before addition of histone H3 and γ-[^{32}P]ATP. (H) Quantification of Aurora B kinase activity as in B (one experiment).

short treatment with OA in the presence or absence of ZM, and examined KT levels of the Ska complex by immunofluorescence. In line with previous measurements in untreated cells (Chan et al., 2012), Ska3 immunofluorescence was approximately twofold higher at metaphase KTs in MG132-arrested cells than at prometaphase KTs in STLC-arrested cells, confirming that the Ska complex accumulates at KTs after biorientation (Fig. 6, A and B). Treatment of prometaphase cells with the phosphatase inhibitor OA had little effect on the KT levels of Ska3, whereas coinhibition of Aurora B with ZM caused an increase of Ska3 staining intensity to levels seen in metaphase control cells (Fig. 6, A and B), confirming that Aurora B activity promotes the dissociation of Ska from KTs in prometaphase (Chan et al., 2012). In striking contrast, phosphatase inhibition by OA in metaphase cells reduced staining of Ska3 at KTs to levels similar to those seen in prometaphase control cells;

furthermore, simultaneous inhibition of Aurora B with ZM reverted this effect, indicating that phosphatase activity counteracts the influence of Aurora B on Ska KT binding (Fig. 6, A and B). Thus, we conclude that either PP2 or PP1 balances Aurora B activity at the outer KT to enable timely enrichment of the Ska complex after chromosome biorientation.

The PP2 family member PP2A has been implicated in regulating the establishment of initial KT-MT contacts (Foley et al., 2011), whereas PP1 has been shown to stabilize attachments by opposing Aurora B activity upon biorientation (Liu et al., 2010). We therefore reasoned that PP1 is most likely to reverse Aurora B phosphorylation of the Ska complex to facilitate its KT association. To test this, we made use of a KNL1 mutant ($KNL1^{RVSF/AAAA}$) devoid of the PP1 binding site, which prevents targeting of PP1 to the outer KT (Liu et al., 2010). Replacement of endogenous KNL1 with $KNL1^{RVSF/AAAA}$ resulted in a loss of Ska3 from KTs to an extent similar to that observed in OA-treated metaphase cells, whereas expression of wild-type KNL1 reverted this effect (Fig. 6, C and D). These results show that PP1 counteracts Aurora B to allow the accumulation of the Ska complex at KTs upon biorientation.

Based on these data, we propose a feedback mechanism in which Ska limits its own enrichment at KTs and/or spindle MTs by promoting Aurora B activity, ensuring a high degree of KT-MT dynamics before establishment of biorientation, whereas PP1 antagonizes this feedback regulation at KTs once biorientation is achieved, allowing Ska, in turn, to stabilize proper K-fiber attachments (Fig. 6 E).

Discussion

In this study, we discovered a novel function of the Ska complex. Specifically, we find that the Ska complex not only is a substrate of Aurora B kinase, but also regulates the activity of this key enzyme. We show that the Ska complex interacts with Aurora B and promotes, in an MT-dependent manner, Aurora B substrate phosphorylation and effector localization as well as Aurora B activation loop phosphorylation in cells. We also demonstrate that Ska directly binds to Aurora B and stimulates its catalytic activity within the CPC core complex in vitro. Furthermore, we reveal hitherto concealed phenotypic aspects of Ska depletion, including suppressed KT-MT plus-end dynamics as well as chromosome biorientation and segregation defects, which distinctly resemble consequences of Aurora B partial loss-of-function. Finally, we demonstrate that PP1 antagonizes Aurora B activity at KTs to enable Ska KT accumulation once biorientation is achieved, which allows the Ska complex to promote K-fiber maturation.

The Ska complex regulates KT-MT dynamics through Aurora B

Our live-cell analysis shows that the Ska complex is required to prevent lagging chromosomes and ensuing micronuclei formation, and it confirms an implication of Ska in chromosome congression, maintenance of chromosome alignment, and timely metaphase-to-anaphase transition—phenotypes that likely reflect different degrees of Ska knockdown (Gaitanos et al., 2009; Welburn et al., 2009). Some of these phenotypes resemble those described for Aurora B inhibition. Specifically, partial inhibition of Aurora B increases, as a result of suppressed KT-MT turnover, the frequency of merotely and lagging chromosomes (Cimini et al., 2006). Our work shows that loss of Ska complex function similarly slows KT-MT turnover, providing an explanation for the appearance of lagging chromosomes and merotelic attachments. Importantly, we find that, along with a lower level of Aurora B T-loop phosphorylation at KTs, phosphorylation of KMN components involved in the regulation of KT-MT attachment stability and KT localization of the MT depolymerase MCAK is perturbed upon Ska depletion, suggesting that Ska acts to mediate KT-MT plus-end dynamics through KMN phosphorylation, regulation of MCAK localization, or both.

Our data further indicate that the Ska complex is required not only for KT-MT plus-end turnover, but also for K-fibers with a normal number of MTs. The latter effect likely mirrors a role of Ska in promoting MT recruitment during K-fiber maturation, by providing additional MT-binding sites within the outer KT (King and Nicklas, 2000), by enhancing the MT-binding affinity of the Ndc80 complex (Schmidt et al., 2012), or both. Moreover, Ska may help to maintain the stability and coherence of MT arrays within K-fibers by laterally cross-linking the lattice of individual MTs at the KT-MT interface. This notion is supported by the findings that the Ska complex has the ability to bundle MTs both in cells and in vitro and that Ska becomes enriched at the KT-MT interface upon chromosome biorientation (Welburn et al., 2009; Chan et al., 2012). Thus, we propose that the Ska complex plays a dual role in the control of KT-MT dynamics via Aurora B and the formation and stabilization of K-fibers and that these functions are linked by a feedback mechanism (discussed later).

Mechanisms of Aurora B regulation by the Ska complex

We found that the Ska complex that localizes to outer KTs and spindle MTs is required for Aurora B phosphorylation of substrates at both KTs and chromosome arms, despite significant centromere levels of Aurora B. Moreover, we observed that forced centromere enrichment of Aurora B did not fully rescue the effect of Ska knockdown on Aurora B activity at KTs and chromosome arms. Finally, we showed that Ska depends on its MT-binding capability to promote Aurora B activity and that MTs, in turn, contribute to Aurora B activation (Banerjee et al., 2014), independently of Aurora B centromeric enrichment. This suggests that control of KT-MT dynamics may depend on a noncentromeric Ska-activated Aurora B pool at KTs or the mitotic spindle (Yue et al., 2008; Tseng et al., 2010; Wang et al., 2012; Campbell and Desai, 2013; Krenn and Musacchio, 2015; Krupina et al., 2016).

Our data further suggest that the Ska complex directly interacts with Aurora B and stimulates, presumably in a Ska1-dependent manner, Aurora B kinase activity. The finding that Ska comparably enhances the catalytic activity of Aurora B regardless of the presence or absence of the INCENP IN-box domain supports the notion that the Ska complex promotes the intrinsic autoactivation capability of Aurora B, possibly by an allosteric mechanism that differs from that of INCENP. Notably, we also observed that histone H3-S10 and H3-S28 phosphorylation levels in cells showed an almost bistable (on/off) response to Ska depletion, whereas other Aurora B activity markers behaved more gradedly (unpublished data). Although we cannot exclude that loss of the Ska complex contributes to suppression of histone H3 tail phosphorylation also independently of Aurora B, this might imply that Ska confers specific substrate recognition properties to Aurora B.

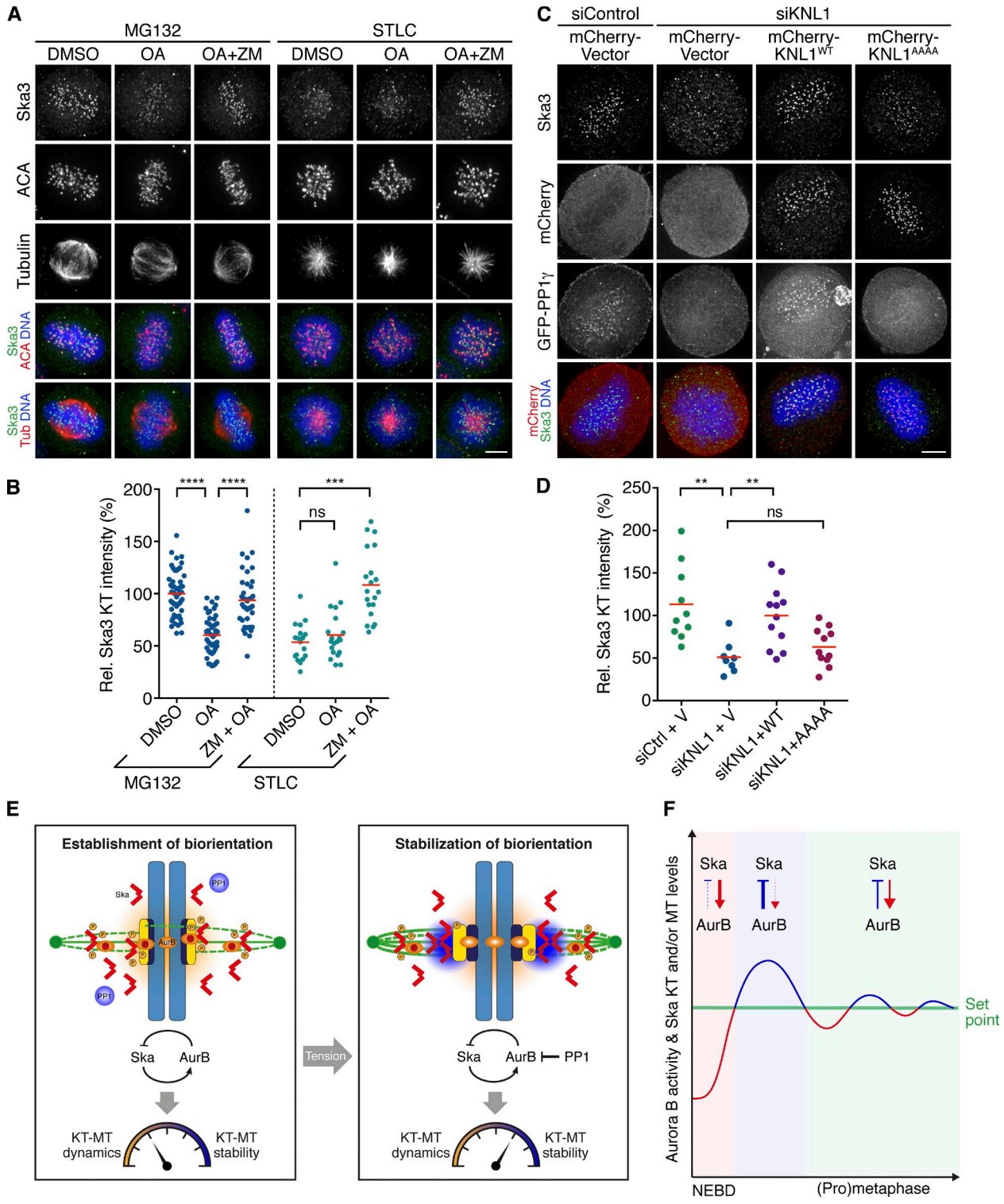

Figure 6. **PP1 opposes Aurora B activity to enable Ska complex enrichment at bioriented KTs.** (A) Asynchronously growing HeLa S3 cells were arrested in metaphase with MG132 (MG) or in early prometaphase with STLC for 2–3 h and treated for 30 min with the indicated combinations of OA and ZM. DMSO treatment served as negative control. Cells were fixed and stained with the indicated antibodies. (B) Quantification of relative Ska3 KT intensities in cells treated as in A (n = 41–51 from two experiments for MG-pretreated cells, and n = 18–20 cells from one experiment for STLC-pretreated cells). (C) HeLa S3 cells were transfected with siRNA-resistant wild-type (WT) mCherry-KNL1 or PP1-binding-deficient mCherry-KNL1$^{RVSF/AAAA}$ together with GFP-PP1γ, before depletion of endogenous KNL1. Cells were fixed and stained with the indicated antibodies. (D) Quantification of relative Ska3 KT intensities in cells treated as in C (n = 8–11 cells per condition from one experiment). (E) Model for the regulation of KT-MT attachment dynamics during chromosome biorientation by the feedback loop between the Ska complex and Aurora B (see Discussion for details). (F) Scheme for feedback control of Ska KT/MT and Aurora B activity levels (see Discussion for details). Horizontal lines depict mean. NEBD, nuclear envelope breakdown. Asterisks show statistical significance (Student's t test, unpaired). ****, $P \leq 0.0001$; ***, $P \leq 0.001$; **, $P \leq 0.01$; ns, nonsignificant. Bars, 5 µm.

Feedback control of chromosome biorientation by the Ska complex

Chromosome biorientation and accurate chromosome segregation rely on the precise control of the attachment stability and dynamics of KT-MTs. Excessively loose or dynamic KT-MT interactions would result in weak K-fiber attachments with an insufficient number of MTs to satisfy the SAC, whereas overly stable or static interactions would prevent maloriented KT-MTs from being replaced efficiently. Our present data identify a Ska–Aurora B feedback loop that contributes to ensure that the attachment stability and dynamics of KT-MTs fall within an optimal balance for efficient chromosome biorientation (Fig. 6 E). According to our model, Ska controls both its own MT and KT association via Aurora B activity (Chan et al., 2012; Schmidt et al., 2012) and, vice versa, Aurora B activity via the extent of its enrichment at MTs and KTs. As Ska levels rapidly rise on spindle MTs and KTs after nuclear envelope breakdown (Hanisch et al., 2006; Raaijmakers et al., 2009), Aurora B activity is driven up. The rise in Aurora B activity, in turn, then increases Ska phosphorylation, which limits further accumulation of Ska at spindle MT and KTs. As a result, both the concentration of the Ska complex on spindle MTs and KTs and the activity of Aurora B level off at a specific set point (Fig. 6 F). It is interesting to note in this context that similar types of feedback loops (where a factor is the activator of a second one, which, in turn, inhibits the first one) are commonly used for temporal control and to dampen fluctuations and balance activities in developmental processes (see for instance the activator/inhibitor pair Nodal/Lefty; Shen, 2007; Schier, 2009; Kondo and Miura, 2010).

Whereas balancing the Ska levels at KTs by Aurora B likely helps to confer a sufficient degree of attachment instability (Chan et al., 2012), limiting Ska-dependent MT cross-linking along the K-fiber lattice may facilitate MT dynamics by reducing the physical constraints on the bending of depolymerizing protofilaments. Restraining Ska MT bundling could also be important to achieve a proper K-fiber organization (Welburn et al., 2009; Nixon et al., 2015). In addition, the Ska-induced increase in Aurora B activity is expected to promote (a) phosphorylation of KMN components, reducing KT-MT attachment stability (Welburn et al., 2010; DeLuca et al., 2011), and/or (b) KT localization of MCAK, which coordinately elevates the MT catastrophe frequencies (Wordeman et al., 2007). Together, these mechanisms aid in maintaining a high KT-MT turnover rate during establishment of biorientation (when attachment errors are most frequently made), which promotes efficient KT reorientation and accumulation of properly attached KT-MTs by exploiting the back-to-back arrangement of sister KTs (Godek et al., 2015; Zaytsev and Grishchuk, 2015).

As bioriented attachments are made, small tension-dependent conformational changes within the KT will allow bulk recruitment of PP1 (Wan et al., 2009; Liu et al., 2010; Posch et al., 2010; Campbell and Desai, 2013; Sarangapani and Asbury, 2014; Suzuki et al., 2014). Upon its targeting to KTs, PP1 would then outweigh the positive influence of Ska on Aurora B activity and the negative influence of Aurora B on Ska, thus permitting the Ska complex to promote further maturation of K-fiber attachments through maximal enrichment at KTs (Fig. 6 E). Interestingly, it has been recently reported that Ska mediates PP1 recruitment to KTs (Sivakumar et al., 2016), which raises the idea that the Ska complex may, like KNL1, coordinate as a signaling hub Aurora B–PP1 activity (Caldas and DeLuca, 2014) to fine-tune the stability and dynamics of K-fiber attachments, in part via its own levels of KT enrichment.

Finally, considering that Aurora B activity remains suppressed in Ska-deficient cells upon chromosome alignment, we consider it likely that stimulation of Aurora B by Ska continues on the spindle in late prometaphase/metaphase. This stimulation could contribute to sustain an appropriate dynamic behavior of KT-MTs for merotelic error correction and chromosome movements.

Materials and methods

Cell culture, transfection, and drug treatments

HeLa S3 and HeLa S3 histone H2B-GFP cells (Silljé et al., 2006) were cultured in DMEM-GlutaMAX supplemented with 10% heat-inactivated FCS, 100 IU/ml penicillin, and 100 mg/ml streptomycin in a humidified incubator at 37°C and 5% CO_2. HeLa K cells stably expressing PA-GFP–α-tubulin/H2B-mRFP or EGFP–CENP-A (Amaro et al., 2010) were further maintained in 250 ng/ml puromycin or 250 ng/ml puromycin and 500 µg/ml G418, respectively. Stable HeLa K H2B-fused Aurora B FRET reporter cells (van der Waal et al., 2012) and HeLa K CENP-B–fused Aurora B FRET reporter cells (gift of D.W. Gerlich, Institute of Molecular Biotechnology, Vienna, Austria) were maintained in 500 ng/ml puromycin. HeLa cells stably expressing siRNA-resistant GFP-Ska1^{WT}, GFP-Ska1$^{R155A, R236A, R245A}$, or GFP-Ska1$^{\Delta MTBD}$ (gift of I.M. Cheeseman, Whitehead Institute, University of California, Berkeley, Berkeley, CA) were cultured as previously described (Schmidt et al., 2012).

Cells were transfected with 50–200 nM siRNAs using Oligofectamine (Invitrogen) and with 0.5 mg/ml plasmid DNA using XtremeGene HP (Roche), according to the manufacturers' instructions. The following siRNA duplexes were used: siSka1-1 (5′-CGCTTAACC TATAATCAAA-3′, used throughout the study unless stated otherwise; Hanisch et al., 2006), siSka3 (5′-AGACAAACATGAACATTAA-3′; Gaitanos et al., 2009), siSka1-2 (5′-GGAGATTTGTGTCAATAAT-3′; Hanisch et al., 2006), siSka2 (5′-GAAATCAAGACTAATCATC-3′; Hanisch et al., 2006), and siKNL1 (5′-GGAATCCAATGCTTTGAGA-3′; Liu et al., 2010). A siRNA duplex targeting luciferase (GL2) served as control: siCtrl (5′-CGTACGCGGAATACTTCGA-3′). The cDNAs of Ska1 and Ska3 were cloned into the pcDNA3.1 vector (Invitrogen), which was modified to carry a single mCherry tag and an N-terminal triple-Myc tag, respectively. For transient rescue experiments, a Ska1 siRNA-resistant version was used (Chan et al., 2012), whereas Ska3 was depleted with an siRNA duplex targeting the 3′ UTR (the sequence reported earlier). Cells were transfected with siRNAs, arrested for 18–20 h with thymidine 24 h after transfection, released into fresh medium for 2 h, and transfected with plasmid DNA, followed by a medium change and a second 16-h thymidine block 4 h after transfection, before being released into fresh medium for 10–11 h, as previously described (Chan et al., 2012). The mCherry-KNL1 wild-type (plasmid #45224; Addgene), mCherry-KNL1$^{RVSF/AAAA}$ mutant (plasmid #45226; Addgene), and GFP-PP1γ constructs were a gift of M. Lampson (University of Pennsylvania, Philadelphia, PA). Rescue experiments with these constructs were performed as previously described (Liu et al., 2010). The plasmid encoding a fusion protein between CENP-B$^{1–158}$ and INCENP$^{48–918}$ in pcDNA3.1 (CB^{DBD}-INCENP; plasmid #45237; Addgene; Wang et al., 2011) was also provided by M. Lampson.

5-Iodotubericidin (Santa Cruz Biotechnology) was used at 10 µM, MG132 (EMD Millipore) at 10 or 20 µM, nocodazole (Sigma-Aldrich) at 3.3 µM, okadaic acid (EMD Millipore) at 1 µM, proTAME (Boston

Biochem) at 20 µM, reversine (Enzo Life Sciences) at 0.5 µM, STLC (Tocris Bioscience) at 10 µM, thymidine (Sigma-Aldrich) at 2 mM, and ZM (Tocris Bioscience) at 5 or 10 µM as indicated in the figures.

Photoactivation assay

Photoactivation experiments were performed in Lab-Tek II chambers (Thermo Fisher Scientific) with Leibovitz L-15 medium containing 10% FCS at 37°C. Photoactivation was performed on bipolar late-prometaphase spindles (identified by the H2B-mRFP signal) as described previously (McHedlishvili et al., 2012). In brief, PA-GFP–α-tubulin was activated in a thin stripe just above the chromosome mass using 150 iterations from a 405-nm laser (100%) on a Zeiss LSM 710-FCS confocal microscope. Fluorescence images were captured every 3 s for 201 s using a 40×/NA1.2 C-Apochromat water objective. Fluorescence intensities were measured in ImageJ at each time frame in circular regions defined by the size of individually activated K-fibers. On average, three to four high signals on different K-fibers in each cell were measured. Background signal was subtracted for each time frame by measuring the same pixel area on the opposite side of the photoactivated spindle. Cells that underwent anaphase in this period were discarded. The values were corrected for photobleaching by determining the fluorescence loss in activated cells treated with 10 µM taxol. The mean data were fitted ($R^2 > 0.99$) to a double-exponential curve, $I = P_{fast} \exp(-k_{fast}\, t) + P_{slow} \exp(-k_{slow}\, t)$, where I is the proportion of the initial fluorescence intensity; P is the proportion of the fluorescence decay caused by the fast or slow process reflecting the fast decaying non-KT-MTs and the more stable KT-MTs with slow turnover, respectively (Zhai et al., 1995); k is the rate constant for the fluorescence decay of the fast or slow process; and t is time. Curve fitting was performed with Prism software (GraphPad). The turnover half-life ($t_{1/2}$) was calculated as $\ln(2)/k$ for each fast and slow process.

Immunofluorescence microscopy, live cell imaging, and FRET

Cells were simultaneously fixed and permeabilized for 10 min at 37°C in PTEMF buffer (20 mM Pipes, pH 6.8, 4% formaldehyde, 0.2% Triton X-100, 10 mM EGTA, and 1 mM $MgCl_2$). For stainings shown in Fig. 2 (A and C) and Fig. S2 (A and B), cells were fixed in PTEMF with 0.5% Triton X-100. For stainings in Figs. 2 I, 3 A, and 4 (E and G), cells were preextracted for 2 min in PEM buffer (100 mM Pipes, pH 6.8, 10 mM EGTA, and 1 mM $MgCl_2$) with 0.4% Triton X-100 at 37°C and then fixed for 10 min at 37°C in 4% formaldehyde in PEM buffer supplemented with 0.2% Triton X-100. Cells were blocked with 3% BSA in PBS for 1 h, incubated with primary antibodies for 12–16 h at 4°C or 1 h at RT, washed with PBS/0.1% Tween 20, and incubated with secondary antibodies and Hoechst dye for an additional 1 h at RT. Primary antibodies used were mouse anti–Aurora B (1:500; AIM-1, 611083, clone 6; BD), rabbit anti–Aurora B–pT232 (1:4,000; 600-401-677; Rockland Immunochemicals), guinea pig anti-mCherry (1:2,000; gift of P. Scheiffele, Biozentrum, Basel, Switzerland), rabbit anti-Dsn1 and anti–Dsn1-pS100 (1:1,000; a gift of I.M. Cheeseman), mouse anti-GFP (1:2,000; ab1218, clone 9F9.F9; Abcam), rabbit anti-GFP (1:1,000; ab290; Abcam), mouse anti-Hec1 (1:2.000; clone 9G3.23; GeneTex), rabbit anti–Hec1-pS44 (1:2,000; gift of J.G. DeLuca, Colorado State University, Fort Collins, CO), rabbit anti–histone H3-pS10 (1:1,000; 06-570; EMD Millipore), rabbit anti–histone H3-pS28 (1:500; 9713P; Cell Signaling Technology), rabbit anti–histone H3-pT3 (1:200; 9714S; Cell Signaling Technology), rabbit anti–KNL1-pS24 (1:2,000; gift of I.M. Cheeseman), rabbit anti-MCAK (1:1,000; Baron et al., 2016), mouse anti-Myc (clone 9E10; Evan et al., 1985), rabbit anti-Ska1 (1:1,000; Hanisch et al., 2006), mouse anti-Ska3 (homemade, described later), and mouse anti–α-tubulin–FITC (1:500; F2168, clone DM1A; Sigma-Aldrich). KTs were identified using human anti-centromere antibodies (ACA; 1:1,000; Immuno Vision), and DNA was stained using Hoechst dye (1:5,000; Thermo Fisher Scientific).

Images were acquired as 15- to 20-µm z-stacks with a step size of 0.4 µm on a DeltaVision system (GE Healthcare) equipped with a 60×/NA1.42 PlanApo N oil objective and a Photometrics CoolSNAP HQ2 camera. Images were deconvolved and projected (maximum-intensity projection) using SoftWorx software (GE Healthcare) and equally scaled using Omero software. Quantifications were performed using an automated pipeline, run by CellProfiler software, which involved the following processing steps: manual selection of mitotic cells, generation of KT/centromere and chromatin masks based on thresholding of pixel intensities of stable KT and chromatin marker signals (ACA and Hoechst, respectively), generation of secondary masks for signal and background measurements (KT/centromere intensity and chromatin intensity), measurement of mean signal intensities per cell within these secondary masks, and export of reference images for quality control of the image segmentation. Measurements of KT/centromere intensities were corrected by subtraction of the mean intensity over the chromatin mask (background) and were normalized over the mean intensity of ACA or background. Signals caused by antibody cross-reactivity to centrosomes were excluded from the measurement masks.

For time-lapse imaging, cells were plated in chambered slides (Lab-Tek II; Ibidi) and filmed in a climate-controlled and humidified environment (37°C and 5% CO_2). High-resolution time-lapse imaging was performed on a DeltaVision system equipped with a 60×/NA1.42 PlanApo N oil objective and a Photometrics CoolSNAP HQ2 camera. Images were captured with 10% neutral density, 10-ms exposure times, and 2× binning in 5-min intervals for 16–18 h with 20 stacks per field spaced 1.5 µm each. Long-term time-lapse imaging was performed on a Nikon Eclipse Ti microscope equipped with a CoolLED pE-1 illumination system and a 20×/NA0.75 Plan Apochromat air objective. Images were captured with 20-ms exposure times in 4-min intervals for 48 h with one stack per field.

FRET experiments were performed on a 3i spinning disk confocal system (Intelligent Imaging Innovations) based on a ZEISS Axio Observer stand equipped with a Photometrics Evolve 512 back-illuminated EMCCD camera, a 63×/NA1.4 Plan Apochromat oil objective, and diode lasers, run by SlideBook software. CFP or TFP was excited with a 440-nm diode laser, and CFP or TFP fluorescence emission (CFP_{em} or TFP_{em}) and YFP ($FRET_{em}$) fluorescence emission was acquired sequentially in z-stacks of 20–30 µm. For the chromatin-targeted sensor, mean CFP and YFP fluorescence intensities were measured in circular regions within the nuclei using ImageJ software, and background-subtracted $CFP_{em}/FRET_{em}$ ratios were calculated and normalized to the mean of all interphase cells of one experimental replicate. For the centromere-targeted sensor, TFP and YFP emissions were aligned by minimizing the mean square difference of intensities between the two images using the StackReg plugin in ImageJ, mean TFP and YFP fluorescence intensities were measured in circular regions defined by the size of individual centromeres using ImageJ, and background-subtracted $TFP_{em}/FRET_{em}$ ratios were calculated.

For both static and live imaging analyses, statistical analyses were done with Prism software (GraphPad).

Protein purification and kinase assays

The plasmid encoding C-terminally His_6-tagged Aurora B was a gift of X. Yao (University of Science and Technology of China, Hefei, China). The open reading frame for Aurora B was sequenced, and a nonsilent point mutation was reverted (R278H) using QuikChange mutagenesis (Agilent Technologies). The cDNA for $INCENP^{790–918}$ was cloned in frame with an N-terminal maltose-binding protein (MBP) tag and a C-terminal His_6 tag into a modified version of the pMAL vector (New

England Biolabs, Inc.). Proteins were expressed in *Escherichia coli* BL21 (DE3), and expression was induced with 0.1 mM IPTG for 4–5 h at 20°C. Aurora B–His_6 was purified under native conditions with Ni-NTA agarose beads (Qiagen) and eluted with 250 mM imidazole. MBP-$INCENP^{790–918}$-His_6 was purified under native conditions with amylose resin (New England Biolabs, Inc.) and eluted with 10 mM maltose, followed by a second purification step with Ni-NTA agarose beads and elution with 250 mM imidazole, according to standard procedures. Proteins were dialyzed against 20 mM Tris, pH 7.4, 100 mM NaCl, 1 mM DTT, and 10% glycerol and concentrated with Amicon Ultra centrifugal filters (EMD Millipore). Protein concentrations were determined by infrared spectrometry using a DirectDetect system (EMD Millipore). Purification of the full-length Ska complex (comprising Ska1-His_6, untagged Ska2, and His_6-Ska3), Ska1-His_6, and His_6-Ska3 has been previously described (Gaitanos et al., 2009; Chan et al., 2012).

For the time course in vitro kinase assays shown in Fig. 5 A and Fig. S5 (B and C), 0.5 µM MBP-$INCENP^{790–918}$-His_6 and 0.5 µM Aurora B–His_6 were preincubated with1 µM recombinant Ska complex, with 1 µM BSA (Sigma-Aldrich) dissolved in Ska complex dialysis buffer (20 mM Tris, pH 7.4, 100 mM NaCl, 1 mM DTT, and 10% glycerol), or Ska complex dialysis buffer without BSA in 25 µl kinase buffer A (25 mM Hepes, pH 7.4, 50 mM NaCl, 1 mM DTT, and 5 mM $MgCl_2$) supplemented with EDTA-free protease inhibitor cocktail (Roche) for 30 min at 30°C. 2 µg recombinant histone H3.1 (New England Biolabs, Inc.), 10 µM ATP, and 5 µCi γ-[^{32}P]ATP were added to a final volume of 30 µl to start the kinase reactions. Reactions were stopped after the indicated incubation times at 30°C by adding 7.5 µl of 5× Laemmli buffer and heating to 95°C. The first time point was pipetted on ice. The time course in vitro kinase assay shown in Fig. S5 H was performed as described earlier in the absence of MBP-$INCENP^{790–918}$-His_6 and recombinant histone H3.1. For the time course assay in Fig. 5 G, 0.5 µM Aurora B–His_6 was preincubated with 0.5 µM BSA, 0.5 µM Ska complex, or 0.5 µM MBP-$INCENP^{790–918}$-His_6 for 30 min at 30°C in kinase buffer A supplemented with EDTA-free protease inhibitor cocktail before addition of 2 µg histone H3.1 (New England Biolabs, Inc.), 10 µM ATP, and 5 µCi γ-[^{32}P]ATP. The first time-point was pipetted on ice. Reactions were stopped after the indicated incubation times at 30°C by adding 7.5 µl of 5× Laemmli buffer and heating to 95°C. For the titration autophosphorylation assays shown in Fig. 5 E and Fig. S5 J, 0.5 µM Aurora B–His_6 was preincubated with histone H3 (as control), Ska complex, Ska1-His_6, or His_6-Ska3 at the indicated concentrations for 30 min at 30°C in kinase buffer A before addition of 10 µM ATP and 5 µCi γ-[^{32}P]ATP. Reactions were stopped after 30 min at 30°C by adding 5× Laemmli buffer and heating to 95°C. For the control assay shown in Fig. S5 D, 0.5 µM Aurora B–His_6 was preincubated with buffer or 1 µM BSA for 30 min at 30°C in kinase buffer A before addition of 10 µM ATP and 5 µCi γ-[^{32}P]ATP, and reactions were stopped after 30 min at 30°C. For the control assay shown in Fig. S5 E, 2 µg histone H3 was incubated with Ska complex dialysis buffer, 1 µM Ska complex, or 1 µM Ska complex and 10 µM ZM for 30 min at 30°C in the presence of γ-[^{32}P]ATP. Kinase reactions were separated by SDS-PAGE, transferred to PVDF membranes, or stained with Coomassie Brilliant Blue, and ^{32}P incorporation was determined by autoradiography and densitometric analysis of the bands using the gel analyzer tool in ImageJ. Curve fittings and statistical analyses were done with Prism software (GraphPad).

Immunoprecipitation and in vitro binding assays

HeLa S3 cells were synchronized with STLC (10 µM) for 16–18 h. Mitotic cells were collected by shake-off and lysed for 20 min at 4°C in IP buffer (20 mM Tris, pH 7.4, 0.5% Triton X-100, 150 mM NaCl, 5 mM $MgCl_2$, 2 mM EGTA, 1 mM DTT, and protease and phosphatase inhibitor cocktail) supplemented with 30 µg/ml DNase and 30 µg/ml RNase. Cell extracts were cleared at 20,000 *g* for 10 min at 4°C. The supernatants (1–2 mg total protein) were incubated for 2–3 h at 4°C with 3 µg anti-Ska1 (Hanisch et al., 2006), 1.5 µg anti–Aurora B (AIM-1, 611083, clone 6; BD), or equivalent amounts of control IgG antibodies, followed by another 1-h incubation with protein G Sepharose beads (GE Healthcare). Alternatively, cell extracts were incubated for 3–4 h with chemically cross-linked anti-INCENP (clone 58-217; EMD Millipore) or control IgG protein G Sepharose beads. The beads were washed five times with IP buffer and boiled in 2× Laemmli buffer.

For in vitro binding assays, 50 nM recombinant Ska complex was incubated for 1 h at 30°C with 100 nM Aurora B–His_6 in binding buffer (20 mM Tris, pH 7.4, 100 mM KCl, 10 mM $MgCl_2$, 1 mM DTT, 1% Triton X-100, and 10% glycerol) before pull-down with chemically cross-linked anti-Ska1 (Hanisch et al., 2006) or IgG protein G Sepharose beads for 2 h at 4°C. Beads were washed five times with PBS and boiled in 2× Laemmli buffer.

Western blotting

Cells were synchronized in mitosis with STLC (10 µM) for 12–16 h and harvested by shake-off. Cells were lysed in extraction buffer (20 mM Tris, pH 7.4, 0.5% Triton X-100, 150 mM NaCl, 5 mM $MgCl_2$, 2 mM EGTA, 1 mM DTT, 30 µg/ml DNase, 30 µg/ml RNase, and protease and phosphatase inhibitor cocktail) or boiled and sonicated in nuclear lysis buffer (20 mM Tris, pH 8, 10 mM EDTA, and 2% SDS). Cell lysates were resolved by SDS-PAGE and transferred to PVDF membranes. The following antibodies were used for Western blotting: mouse anti–Aurora B (1:500; AIM-1, 611083, clone 6; BD), mouse anti-His_4 (1:2,000; 34670; Qiagen), rabbit anti-INCENP (1:500; Honda et al., 2003), rabbit anti-MCAK (1:1,000; Baron et al., 2016), mouse anti-MBP (1:10,000; E8032; New England Biolabs, Inc.), rabbit anti-Ska1 and anti-Ska2 (1:1,000; Hanisch et al., 2006), rabbit anti-Ska3 (1:1,000; Gaitanos et al., 2009), rabbit anti-Survivin (1:1,000; NB500-201; Novus Biologicals), and mouse anti–α-tubulin (1:3,000; T6199, clone DM1A; Sigma-Aldrich).

Monoclonal antibody production

Novel monoclonal antibodies against Ska3 were developed commercially with Moravian Biotechnology. The antibodies (IgG_1) were generated against His-tagged full-length human Ska complex reconstituted from *E. coli* as previously described (Gaitanos et al., 2009; Chan et al., 2012). Repeated intraperitoneal injections of 10–50 µg antigen into BALB/c mice were performed using Freund's adjuvant. Splenocytes where fused with SP2 myeloma cells. Supernatant screening was performed by ELISA.

Online supplemental material

Fig. S1 shows additional consequences of Ska complex depletion on mitotic fidelity, prevalence of merotelic KTs in Ska-depleted cells, comparable Ska1 knockdown efficiencies in HeLa S3 and HeLa K cells upon double and single siRNA treatment, respectively, and confirmation of the effects of Ska complex depletion on KT-MT dynamics with a siRNA against an alternative Ska complex subunit. Fig. S2 shows reduced Dsn1-pS100 and H3-pS28 levels in Ska-depleted cells, confirmation of the effect of Ska depletion on H3-pS10 with a panel of alternative siRNAs, and the FRET data from Fig. 2 (L and N) normalized to control and ZM cells. Fig. S3 shows that CPC protein levels and complex formation remain unaffected in Ska-depleted cells, that neither cohesion fatigue nor Haspin kinase inhibition impairs H3-S10 phosphorylation despite displacement of centromeric Aurora B, and that MCAK KT and H3-pS10 levels are not restored after ectopic centromere enrichment of Aurora B in the absence of

Ska. Fig. S4 shows GFP-Ska1 fusion protein levels at KTs in the stable cell lines used in Fig. 4 and the dependence of Aurora B activity toward H3-S10 on spindle MTs. Fig. S5 shows purification of recombinant proteins used for in vitro kinase assays in Fig. 5 and additional control experiments related to Fig. 5. Table S1 shows the double exponential decay curve fitting parameters and sample sizes analyzed, related to Fig. 1 (F–I).

Acknowledgments

We are grateful to I.M. Cheeseman, J.G. DeLuca, D.W. Gerlich, A.A. Jeyaprakash, M.A. Abad, M. Lampson, P. Scheiffele, and X. Yao for sharing cell lines and reagents. We acknowledge the Imaging Core Facility of the Biozentrum and the Light Microscopy Centre of the Swiss Federal Institute of Technology in Zurich for microscopy support and further thank C. von Schubert for initial help with FRET sensor imaging.

This work was supported by the Universität Basel as well as by grants from the Krebsliga Schweiz (KFS 02657-08-2010 to A. Santamaria and E.A. Nigg) and the Schweizerischer Nationalfonds zur Förderung der Wissenschaftlichen Forschung (310030B-149641 to E.A. Nigg). A. Santamaria is currently supported by the Miguel Servet Program from the Instituto de Salud Carlos III (CP13/00158), cofunded by the European Regional Development Fund. P. Meraldi and I. Gasic were supported by the Université de Genève and the Schweizerischer Nationalfonds zur Förderung der Wissenschaftlichen Forschung (SNF 31003A_141256); I. Gasic was a Boehringer Ingelheim fellow.

The authors declare no competing financial interests.

Submitted: 6 March 2016
Accepted: 31 August 2016

References

Abad, M.A., B. Medina, A. Santamaria, J. Zou, C. Plasberg-Hill, A. Madhumalar, U. Jayachandran, P.M. Redli, J. Rappsilber, E.A. Nigg, and A.A. Jeyaprakash. 2014. Structural basis for microtubule recognition by the human kinetochore Ska complex. *Nat. Commun.* 5:2964. http://dx.doi.org/10.1038/ncomms3964

Amaro, A.C., C.P. Samora, R. Holtackers, E. Wang, I.J. Kingston, M. Alonso, M. Lampson, A.D. McAinsh, and P. Meraldi. 2010. Molecular control of kinetochore-microtubule dynamics and chromosome oscillations. *Nat. Cell Biol.* 12:319–329. http://dx.doi.org/10.1038/ncb2033

Andrews, P.D., Y. Ovechkina, N. Morrice, M. Wagenbach, K. Duncan, L. Wordeman, and J.R. Swedlow. 2004. Aurora B regulates MCAK at the mitotic centromere. *Dev. Cell.* 6:253–268. http://dx.doi.org/10.1016/S1534-5807(04)00025-5

Bakhoum, S.F., and D.A. Compton. 2012. Kinetochores and disease: Keeping microtubule dynamics in check! *Curr. Opin. Cell Biol.* 24:64–70. http://dx.doi.org/10.1016/j.ceb.2011.11.012

Bakhoum, S.F., S.L. Thompson, A.L. Manning, and D.A. Compton. 2009. Genome stability is ensured by temporal control of kinetochore-microtubule dynamics. *Nat. Cell Biol.* 11:27–35. http://dx.doi.org/10.1038/ncb1809

Banerjee, B., C.A. Kestner, and P.T. Stukenberg. 2014. EB1 enables spindle microtubules to regulate centromeric recruitment of Aurora B. *J. Cell Biol.* 204:947–963. http://dx.doi.org/10.1083/jcb.201307119

Baron, A.P., C. von Schubert, F. Cubizolles, G. Siemeister, M. Hitchcock, A. Mengel, J. Schröder, A. Fernández-Montalván, F. von Nussbaum, D. Mumberg, and E.A. Nigg. 2016. Probing the catalytic functions of Bub1 kinase using the small molecule inhibitors BAY-320 and BAY-524. *eLife.* 5:e12187. http://dx.doi.org/10.7554/eLife.12187

Bekier, M.E., T. Mazur, M.S. Rashid, and W.R. Taylor. 2015. Borealin dimerization mediates optimal CPC checkpoint function by enhancing localization to centromeres and kinetochores. *Nat. Commun.* 6:6775. http://dx.doi.org/10.1038/ncomms7775

Caldas, G.V., and J.G. DeLuca. 2014. KNL1: Bringing order to the kinetochore. *Chromosoma.* 123:169–181. http://dx.doi.org/10.1007/s00412-013-0446-5

Campbell, C.S., and A. Desai. 2013. Tension sensing by Aurora B kinase is independent of survivin-based centromere localization. *Nature.* 497:118–121. http://dx.doi.org/10.1038/nature12057

Carmena, M., M. Wheelock, H. Funabiki, and W.C. Earnshaw. 2012. The chromosomal passenger complex (CPC): From easy rider to the godfather of mitosis. *Nat. Rev. Mol. Cell Biol.* 13:789–803. http://dx.doi.org/10.1038/nrm3474

Chan, Y.W., A.A. Jeyaprakash, E.A. Nigg, and A. Santamaria. 2012. Aurora B controls kinetochore-microtubule attachments by inhibiting Ska complex-KMN network interaction. *J. Cell Biol.* 196:563–571. http://dx.doi.org/10.1083/jcb.201109001

Cheeseman, I.M., J.S. Chappie, E.M. Wilson-Kubalek, and A. Desai. 2006. The conserved KMN network constitutes the core microtubule-binding site of the kinetochore. *Cell.* 127:983–997. http://dx.doi.org/10.1016/j.cell.2006.09.039

Cimini, D., B. Howell, P. Maddox, A. Khodjakov, F. Degrassi, and E.D. Salmon. 2001. Merotelic kinetochore orientation is a major mechanism of aneuploidy in mitotic mammalian tissue cells. *J. Cell Biol.* 153:517–527. http://dx.doi.org/10.1083/jcb.153.3.517

Cimini, D., D. Fioravanti, E.D. Salmon, and F. Degrassi. 2002. Merotelic kinetochore orientation versus chromosome mono-orientation in the origin of lagging chromosomes in human primary cells. *J. Cell Sci.* 115:507–515.

Cimini, D., X. Wan, C.B. Hirel, and E.D. Salmon. 2006. Aurora kinase promotes turnover of kinetochore microtubules to reduce chromosome segregation errors. *Curr. Biol.* 16:1711–1718. http://dx.doi.org/10.1016/j.cub.2006.07.022

Daum, J.R., J.D. Wren, J.J. Daniel, S. Sivakumar, J.N. McAvoy, T.A. Potapova, and G.J. Gorbsky. 2009. Ska3 is required for spindle checkpoint silencing and the maintenance of chromosome cohesion in mitosis. *Curr. Biol.* 19:1467–1472. http://dx.doi.org/10.1016/j.cub.2009.07.017

De Antoni, A., S. Maffini, S. Knapp, A. Musacchio, and S. Santaguida. 2012. A small-molecule inhibitor of Haspin alters the kinetochore functions of Aurora B. *J. Cell Biol.* 199:269–284. http://dx.doi.org/10.1083/jcb.201205119

DeLuca, J.G., W.E. Gall, C. Ciferri, D. Cimini, A. Musacchio, and E.D. Salmon. 2006. Kinetochore microtubule dynamics and attachment stability are regulated by Hec1. *Cell.* 127:969–982. http://dx.doi.org/10.1016/j.cell.2006.09.047

DeLuca, K.F., S.M.A. Lens, and J.G. DeLuca. 2011. Temporal changes in Hec1 phosphorylation control kinetochore-microtubule attachment stability during mitosis. *J. Cell Sci.* 124:622–634. http://dx.doi.org/10.1242/jcs.072629

Ditchfield, C., V.L. Johnson, A. Tighe, R. Ellston, C. Haworth, T. Johnson, A. Mortlock, N. Keen, and S.S. Taylor. 2003. Aurora B couples chromosome alignment with anaphase by targeting BubR1, Mad2, and Cenp-E to kinetochores. *J. Cell Biol.* 161:267–280. http://dx.doi.org/10.1083/jcb.200208091

Evan, G.I., G.K. Lewis, G. Ramsay, and J.M. Bishop. 1985. Isolation of monoclonal antibodies specific for human c-myc proto-oncogene product. *Mol. Cell. Biol.* 5:3610–3616. http://dx.doi.org/10.1128/MCB.5.12.3610

Foley, E.A., M. Maldonado, and T.M. Kapoor. 2011. Formation of stable attachments between kinetochores and microtubules depends on the B56-PP2A phosphatase. *Nat. Cell Biol.* 13:1265–1271. http://dx.doi.org/10.1038/ncb2327

Francisco, L., W. Wang, and C.S.M. Chan. 1994. Type 1 protein phosphatase acts in opposition to IpL1 protein kinase in regulating yeast chromosome segregation. *Mol. Cell. Biol.* 14:4731–4740. http://dx.doi.org/10.1128/MCB.14.7.4731

Fuller, B.G., M.A. Lampson, E.A. Foley, S. Rosasco-Nitcher, K.V. Le, P. Tobelmann, D.L. Brautigan, P.T. Stukenberg, and T.M. Kapoor. 2008. Midzone activation of aurora B in anaphase produces an intracellular phosphorylation gradient. *Nature.* 453:1132–1136. http://dx.doi.org/10.1038/nature06923

Gaitanos, T.N., A. Santamaria, A.A. Jeyaprakash, B. Wang, E. Conti, and E.A. Nigg. 2009. Stable kinetochore-microtubule interactions depend on the Ska complex and its new component Ska3/C13Orf3. *EMBO J.* 28:1442–1452. http://dx.doi.org/10.1038/emboj.2009.96

Godek, K.M., L. Kabeche, and D.A. Compton. 2015. Regulation of kinetochore-microtubule attachments through homeostatic control during mitosis. *Nat. Rev. Mol. Cell Biol.* 16:57–64. http://dx.doi.org/10.1038/nrm3916

Goto, H., Y. Yasui, E.A. Nigg, and M. Inagaki. 2002. Aurora-B phosphorylates Histone H3 at serine28 with regard to the mitotic chromosome condensation. *Genes Cells.* 7:11–17. http://dx.doi.org/10.1046/j.1356-9597.2001.00498.x

Hanisch, A., H.H.W. Silljé, and E.A. Nigg. 2006. Timely anaphase onset requires a novel spindle and kinetochore complex comprising Ska1 and Ska2. *EMBO J.* 25:5504–5515. http://dx.doi.org/10.1038/sj.emboj.7601426

Hauf, S., R.W. Cole, S. LaTerra, C. Zimmer, G. Schnapp, R. Walter, A. Heckel, J. van Meel, C.L. Rieder, and J.-M. Peters. 2003. The small molecule Hesperadin reveals a role for Aurora B in correcting kinetochore-microtubule attachment and in maintaining the spindle assembly checkpoint. *J. Cell Biol.* 161:281–294. http://dx.doi.org/10.1083/jcb.200208092

Honda, R., R. Körner, and E.A. Nigg. 2003. Exploring the functional interactions between Aurora B, INCENP, and survivin in mitosis. *Mol. Biol. Cell.* 14:3325–3341. http://dx.doi.org/10.1091/mbc.E02-11-0769

Hsu, J.Y., Z.W. Sun, X. Li, M. Reuben, K. Tatchell, D.K. Bishop, J.M. Grushcow, C.J. Brame, J.A. Caldwell, D.F. Hunt, et al. 2000. Mitotic phosphorylation of histone H3 is governed by Ipl1/aurora kinase and Glc7/PP1 phosphatase in budding yeast and nematodes. *Cell.* 102:279–291. http://dx.doi.org/10.1016/S0092-8674(00)00034-9

Jeyaprakash, A.A., A. Santamaria, U. Jayachandran, Y.W. Chan, C. Benda, E.A. Nigg, and E. Conti. 2012. Structural and functional organization of the Ska complex, a key component of the kinetochore-microtubule interface. *Mol. Cell.* 46:274–286. http://dx.doi.org/10.1016/j.molcel.2012.03.005

Kelly, A.E., S.C. Sampath, T.A. Maniar, E.M. Woo, B.T. Chait, and H. Funabiki. 2007. Chromosomal enrichment and activation of the aurora B pathway are coupled to spatially regulate spindle assembly. *Dev. Cell.* 12:31–43. http://dx.doi.org/10.1016/j.devcel.2006.11.001

Kelly, A.E., C. Ghenoiu, J.Z. Xue, C. Zierhut, H. Kimura, and H. Funabiki. 2010. Survivin reads phosphorylated histone H3 threonine 3 to activate the mitotic kinase Aurora B. *Science.* 330:235–239. http://dx.doi.org/10.1126/science.1189505

King, J.M., and R.B. Nicklas. 2000. Tension on chromosomes increases the number of kinetochore microtubules but only within limits. *J. Cell Sci.* 113:3815–3823.

Kondo, S., and T. Miura. 2010. Reaction-diffusion model as a framework for understanding biological pattern formation. *Science.* 329:1616–1620. http://dx.doi.org/10.1126/science.1179047

Krenn, V., and A. Musacchio. 2015. The Aurora B kinase in chromosome bi-orientation and spindle checkpoint signaling. *Front. Oncol.* 5:225. http://dx.doi.org/10.3389/fonc.2015.00225

Krupina, K., C. Kleiss, T. Metzger, S. Fournane, S. Schmucker, K. Hofmann, B. Fischer, N. Paul, I.M. Porter, W. Raffelsberger, et al. 2016. Ubiquitin receptor protein UBASH3B drives Aurora B recruitment to mitotic microtubules. *Dev. Cell.* 36:63–78. http://dx.doi.org/10.1016/j.devcel.2015.12.017

Lampson, M.A., K. Renduchitala, A. Khodjakov, and T.M. Kapoor. 2004. Correcting improper chromosome-spindle attachments during cell division. *Nat. Cell Biol.* 6:232–237. http://dx.doi.org/10.1038/ncb1102

Lan, W., X. Zhang, S.L. Kline-Smith, S.E. Rosasco, G.A. Barrett-Wilt, J. Shabanowitz, D.F. Hunt, C.E. Walczak, and P.T. Stukenberg. 2004. Aurora B phosphorylates centromeric MCAK and regulates its localization and microtubule depolymerization activity. *Curr. Biol.* 14:273–286. http://dx.doi.org/10.1016/j.cub.2004.01.055

Lengauer, C., K.W. Kinzler, and B. Vogelstein. 1998. Genetic instabilities in human cancers. *Nature.* 396:643–649. http://dx.doi.org/10.1038/25292

Liu, D., G. Vader, M.J.M. Vromans, M.A. Lampson, and S.M.A. Lens. 2009. Sensing chromosome bi-orientation by spatial separation of aurora B kinase from kinetochore substrates. *Science.* 323:1350–1353. http://dx.doi.org/10.1126/science.1167000

Liu, D., M. Vleugel, C.B. Backer, T. Hori, T. Fukagawa, I.M. Cheeseman, and M.A. Lampson. 2010. Regulated targeting of protein phosphatase 1 to the outer kinetochore by KNL1 opposes Aurora B kinase. *J. Cell Biol.* 188:809–820. http://dx.doi.org/10.1083/jcb.201001006

McHedlishvili, N., S. Wieser, R. Holtackers, J. Mouysset, M. Belwal, A.C. Amaro, and P. Meraldi. 2012. Kinetochores accelerate centrosome separation to ensure faithful chromosome segregation. *J. Cell Sci.* 125:906–918. http://dx.doi.org/10.1242/jcs.091967

Muñoz-Barrera, M., and F. Monje-Casas. 2014. Increased Aurora B activity causes continuous disruption of kinetochore-microtubule attachments and spindle instability. *Proc. Natl. Acad. Sci. USA.* 111:E3996–E4005. http://dx.doi.org/10.1073/pnas.1408017111

Nixon, F.M., C. Gutiérrez-Caballero, F.E. Hood, D.G. Booth, I.A. Prior, and S.J. Royle. 2015. The mesh is a network of microtubule connectors that stabilizes individual kinetochore fibers of the mitotic spindle. *eLife.* 4:1–44. http://dx.doi.org/10.7554/eLife.07635

Petsalaki, E., T. Akoumianaki, E.J. Black, D.A.F. Gillespie, and G. Zachos. 2011. Phosphorylation at serine 331 is required for Aurora B activation. *J. Cell Biol.* 195:449–466. http://dx.doi.org/10.1083/jcb.201104023

Posch, M., G.A. Khoudoli, S. Swift, E.M. King, J.G. Deluca, and J.R. Swedlow. 2010. Sds22 regulates aurora B activity and microtubule-kinetochore interactions at mitosis. *J. Cell Biol.* 191:61–74. http://dx.doi.org/10.1083/jcb.200912046

Raaijmakers, J.A., M.E. Tanenbaum, A.F. Maia, and R.H. Medema. 2009. RAMA1 is a novel kinetochore protein involved in kinetochore-microtubule attachment. *J. Cell Sci.* 122:2436–2445. http://dx.doi.org/10.1242/jcs.051912

Rosasco-Nitcher, S.E., W. Lan, S. Khorasanizadeh, and P.T. Stukenberg. 2008. Centromeric Aurora-B activation requires TD-60, microtubules, and substrate priming phosphorylation. *Science.* 319:469–472. http://dx.doi.org/10.1126/science.1148980

Salmon, E.D., D. Cimini, L.A. Cameron, and J.G. DeLuca. 2005. Merotelic kinetochores in mammalian tissue cells. *Philos. Trans. R. Soc. Lond. B Biol. Sci.* 360:553–568. http://dx.doi.org/10.1098/rstb.2004.1610

Sarangapani, K.K., and C.L. Asbury. 2014. Catch and release: How do kinetochores hook the right microtubules during mitosis? *Trends Genet.* 30:150–159. http://dx.doi.org/10.1016/j.tig.2014.02.004

Sarangapani, K.K., B. Akiyoshi, N.M. Duggan, S. Biggins, and C.L. Asbury. 2013. Phosphoregulation promotes release of kinetochores from dynamic microtubules via multiple mechanisms. *Proc. Natl. Acad. Sci. USA.* 110:7282–7287. http://dx.doi.org/10.1073/pnas.1220700110

Schier, A.F. 2009. Nodal morphogens. *Cold Spring Harb. Perspect. Biol.* 1:a003459. http://dx.doi.org/10.1101/cshperspect.a003459

Schmidt, J.C., H. Arthanari, A. Boeszoermenyi, N.M. Dashkevich, E.M. Wilson-Kubalek, N. Monnier, M. Markus, M. Oberer, R.A. Milligan, M. Bathe, et al. 2012. The kinetochore-bound Ska1 complex tracks depolymerizing microtubules and binds to curved protofilaments. *Dev. Cell.* 23:968–980. http://dx.doi.org/10.1016/j.devcel.2012.09.012

Shen, M.M. 2007. Nodal signaling: Developmental roles and regulation. *Development.* 134:1023–1034. http://dx.doi.org/10.1242/dev.000166

Silljé, H.H.W., S. Nagel, R. Körner, and E.A. Nigg. 2006. HURP is a Ran-importin β-regulated protein that stabilizes kinetochore microtubules in the vicinity of chromosomes. *Curr. Biol.* 16:731–742. http://dx.doi.org/10.1016/j.cub.2006.02.070

Sivakumar, S., J.R. Daum, A.R. Tipton, S. Rankin, and G.J. Gorbsky. 2014. The spindle and kinetochore-associated (Ska) complex enhances binding of the anaphase-promoting complex/cyclosome (APC/C) to chromosomes and promotes mitotic exit. *Mol. Biol. Cell.* 25:594–605. http://dx.doi.org/10.1091/mbc.E13-07-0421

Sivakumar, S., P.Ł. Janczyk, Q. Qu, C.A. Brautigam, P.T. Stukenberg, H. Yu, G.J. Gorbsky, and S. Biggins. 2016. The human SKA complex drives the metaphase-anaphase cell cycle transition by recruiting protein phosphatase 1 to kinetochores. *eLife.* 5:e12902–e12920. http://dx.doi.org/10.7554/eLife.12902

Suzuki, A., B.L. Badger, X. Wan, J.G. DeLuca, and E.D. Salmon. 2014. The architecture of CCAN proteins creates a structural integrity to resist spindle forces and achieve proper Intrakinetochore stretch. *Dev. Cell.* 30:717–730. http://dx.doi.org/10.1016/j.devcel.2014.08.003

Tanno, Y., T.S. Kitajima, T. Honda, Y. Ando, K. Ishiguro, and Y. Watanabe. 2010. Phosphorylation of mammalian Sgo2 by Aurora B recruits PP2A and MCAK to centromeres. *Genes Dev.* 24:2169–2179. http://dx.doi.org/10.1101/gad.1945310

Thompson, S.L., and D.A. Compton. 2011. Chromosome missegregation in human cells arises through specific types of kinetochore-microtubule attachment errors. *Proc. Natl. Acad. Sci. USA.* 108:17974–17978. http://dx.doi.org/10.1073/pnas.1109720108

Thompson, S.L., S.F. Bakhoum, and D.A. Compton. 2010. Mechanisms of chromosomal instability. *Curr. Biol.* 20:R285–R295. http://dx.doi.org/10.1016/j.cub.2010.01.034

Tseng, B.S., L. Tan, T.M. Kapoor, and H. Funabiki. 2010. Dual detection of chromosomes and microtubules by the chromosomal passenger complex drives spindle assembly. *Dev. Cell.* 18:903–912. http://dx.doi.org/10.1016/j.devcel.2010.05.018

Umbreit, N.T., D.R. Gestaut, J.F. Tien, B.S. Vollmar, T. Gonen, C.L. Asbury, and T.N. Davis. 2012. The Ndc80 kinetochore complex directly modulates microtubule dynamics. *Proc. Natl. Acad. Sci. USA.* 109:16113–16118. http://dx.doi.org/10.1073/pnas.1209615109

van der Waal, M.S., A.T. Saurin, M.J.M. Vromans, M. Vleugel, C. Wurzenberger, D.W. Gerlich, R.H. Medema, G.J.P.L. Kops, and S.M.A. Lens. 2012. Mps1 promotes rapid centromere accumulation of Aurora B. *EMBO Rep.* 13:847–854. http://dx.doi.org/10.1038/embor.2012.93

Wan, X., R.P. O'Quinn, H.L. Pierce, A.P. Joglekar, W.E. Gall, J.G. DeLuca, C.W. Carroll, S.-T. Liu, T.J. Yen, B.F. McEwen, et al. 2009. Protein architecture of the human kinetochore microtubule attachment site. *Cell.* 137:672–684. http://dx.doi.org/10.1016/j.cell.2009.03.035

Wang, E., E.R. Ballister, and M.A. Lampson. 2011. Aurora B dynamics at centromeres create a diffusion-based phosphorylation gradient. *J. Cell Biol.* 194:539–549. http://dx.doi.org/10.1083/jcb.201103044

Wang, F., N.P. Ulyanova, J.R. Daum, D. Patnaik, A.V. Kateneva, G.J. Gorbsky, and J.M.G. Higgins. 2012. Haspin inhibitors reveal centromeric functions of Aurora B in chromosome segregation. *J. Cell Biol.* 199:251–268. http://dx.doi.org/10.1083/jcb.201205106

Welburn, J.P.I., E.L. Grishchuk, C.B. Backer, E.M. Wilson-Kubalek, J.R. Yates III, and I.M. Cheeseman. 2009. The human kinetochore Ska1 complex facilitates microtubule depolymerization-coupled motility. *Dev. Cell.* 16:374–385. http://dx.doi.org/10.1016/j.devcel.2009.01.011

Welburn, J.P.I., M. Vleugel, D. Liu, J.R. Yates III, M.A. Lampson, T. Fukagawa, and I.M. Cheeseman. 2010. Aurora B phosphorylates spatially distinct targets to differentially regulate the kinetochore-microtubule interface. *Mol. Cell.* 38:383–392. http://dx.doi.org/10.1016/j.molcel.2010.02.034

Wordeman, L., M. Wagenbach, and G. von Dassow. 2007. MCAK facilitates chromosome movement by promoting kinetochore microtubule turnover. *J. Cell Biol.* 179:869–879. http://dx.doi.org/10.1083/jcb.200707120

Yasui, Y., T. Urano, A. Kawajiri, K. Nagata, M. Tatsuka, H. Saya, K. Furukawa, T. Takahashi, I. Izawa, and M. Inagaki. 2004. Autophosphorylation of a newly identified site of Aurora-B is indispensable for cytokinesis. *J. Biol. Chem.* 279:12997–13003. http://dx.doi.org/10.1074/jbc.M311128200

Yue, Z., A. Carvalho, Z. Xu, X. Yuan, S. Cardinale, S. Ribeiro, F. Lai, H. Ogawa, E. Gudmundsdottir, R. Gassmann, et al. 2008. Deconstructing Survivin: Comprehensive genetic analysis of Survivin function by conditional knockout in a vertebrate cell line. *J. Cell Biol.* 183:279–296. http://dx.doi.org/10.1083/jcb.200806118

Zaytsev, A.V., and E.L. Grishchuk. 2015. Basic mechanism for biorientation of mitotic chromosomes is provided by the kinetochore geometry and indiscriminate turnover of kinetochore microtubules. *Mol. Biol. Cell.* 26:3985–3998. http://dx.doi.org/10.1091/mbc.E15-06-0384

Zhai, Y., P.J. Kronebusch, and G.G. Borisy. 1995. Kinetochore microtubule dynamics and the metaphase-anaphase transition. *J. Cell Biol.* 131:721–734. http://dx.doi.org/10.1083/jcb.131.3.721